PONTICULUS POSTICUS

Negli esseri umani il *ponticulus posticus* è descritto come *variazione* anatomica; nei quadrupedi è considerato normale dove ha probabilmente un significato funzionale (*protezione arteria vertebrale*)

Nell'uomo postura eretta e carico della testa sull'atlante hanno portato alla scomparsa del pp

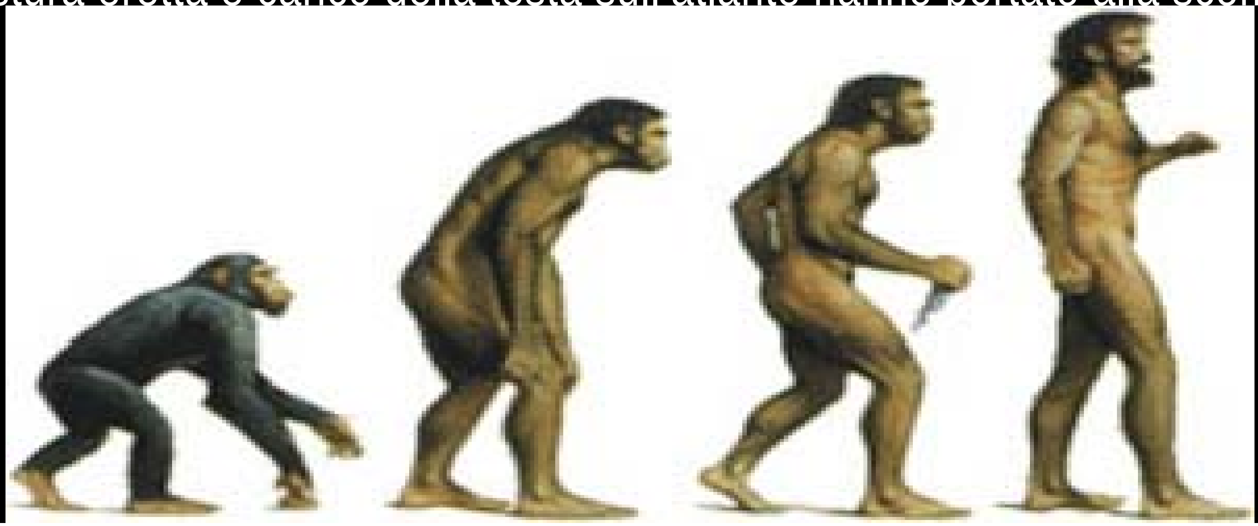

WHY WE NEED GENOMIC ANTHROPOLOGY IN ORTHODONTICS?

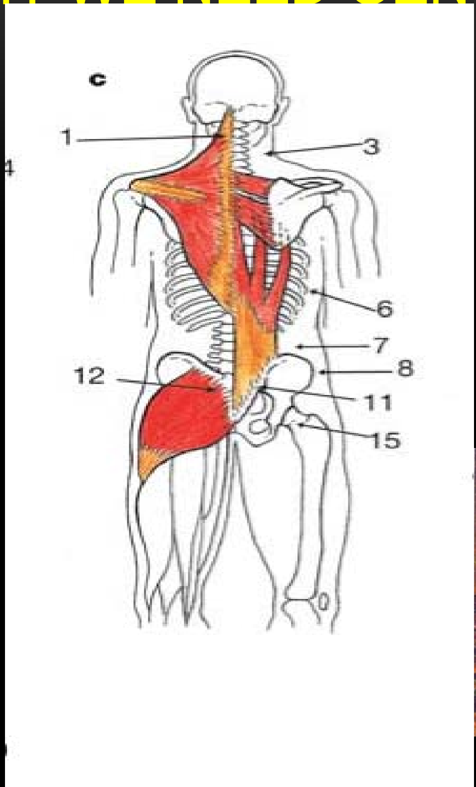

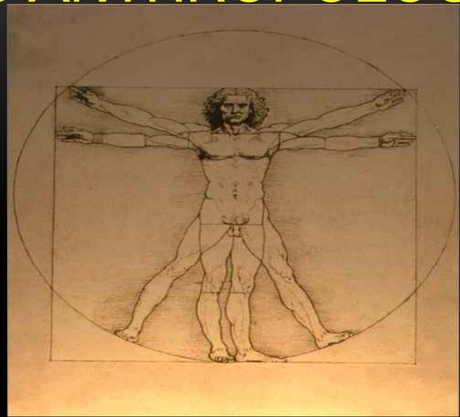

?

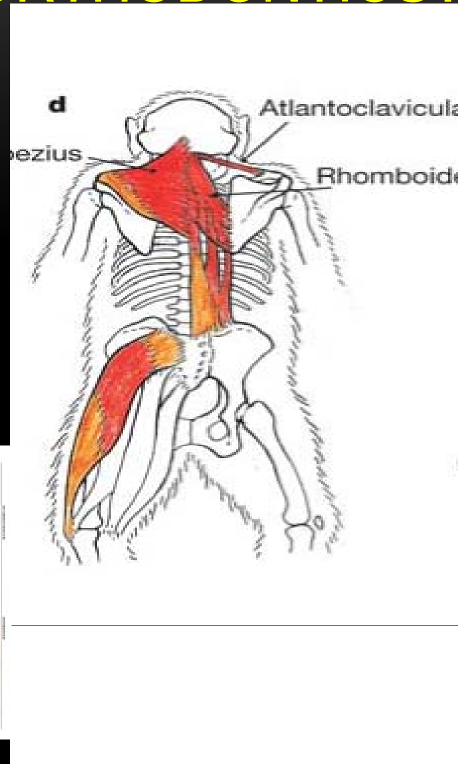

BECAUSE WE HAVE ~~A BAD ADAPTATION TO UPRIGHT~~ POSTURE

© 2015. Published by The Company of Biologists Ltd | The Journal of Experimental Biology (2015) 218, 2382-2393 doi:10.1242/jeb.117952

RESEARCH ARTICLE

The human iliotibial band is specialized for elastic energy storage compared with the chimp fascia lata

Carolyn M. Eng[1,2,*], Allison S. Arnold[1], Andrew A. Biewener[1] and Daniel E. Lieberman[2]

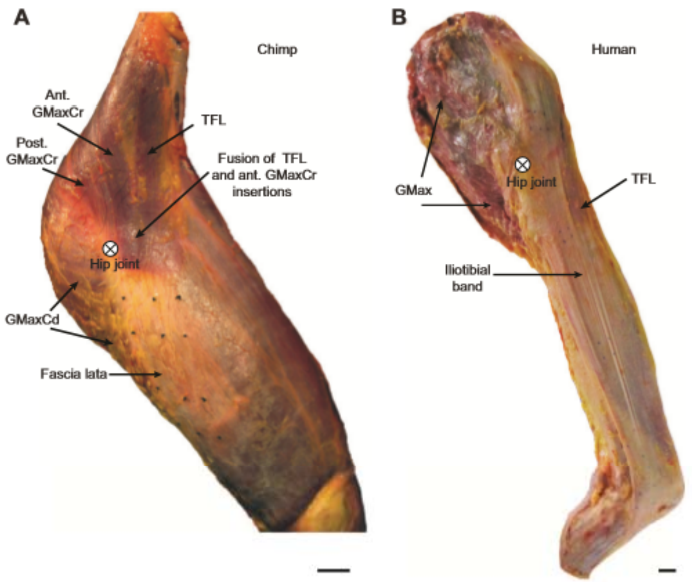

Fig. 1. Lateral view of the chimpanzee and human lower limbs. (A) The chimp limb shows the distal fusion of the TFL and anterior GMaxCr muscle fibers proximal to where they insert in the anterior FL. The posterior GMaxCr fibers insert in the lateral femur. The superficial GMaxCd fibers insert in the posterior FL. The locations of suture marker pairs (visible as black dots) in the anterior and posterior FL were tracked with high-speed video and used to determine the hip and knee angles at which the anterior and posterior FL began to stretch. (B) In the human limb, TFL inserts in the anterior ITB, while a portion of GMax fibers inserts in the posterior ITB. Although the human GMax is homologous to the chimp GMaxCr, GMax–ITB_{post} energy storage was compared with GMaxCd–FL_{post} energy storage because of the posterior insertions of the muscles and similar hip extension moment arms. Scale bars: 2 cm.

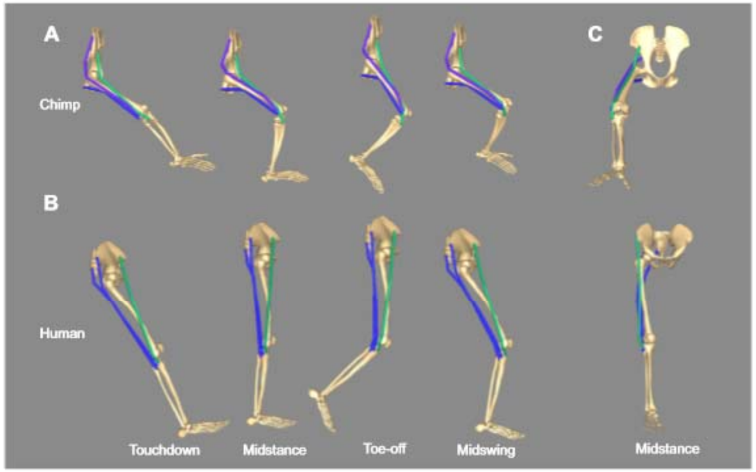

Fig. 2. Chimpanzee and human lower extremity models during bipedal walking. (A) Lateral view of the chimp model modified from O'Neill et al. (2013) showing FL MTUs including TFL–FL_{ant} (green), GMaxCr–FL_{ant} (purple) and GMaxCd–FL_{post} (blue) during touchdown, midstance, toe-off and midswing during bipedal walking. (B) Lateral view of the human model from Eng et al. (2015) showing ITB MTUs including TFL–ITB_{ant} (green) and GMax–ITB_{post} (blue) during bipedal walking. The human GMax–ITB_{post} MTU is color-coded based on its insertion in the posterior ITB and not based on homology. (C) Anterior view of the chimp (top) and human (bottom) models during midstance, showing the abducted position of the chimp hip during bipedal walking.

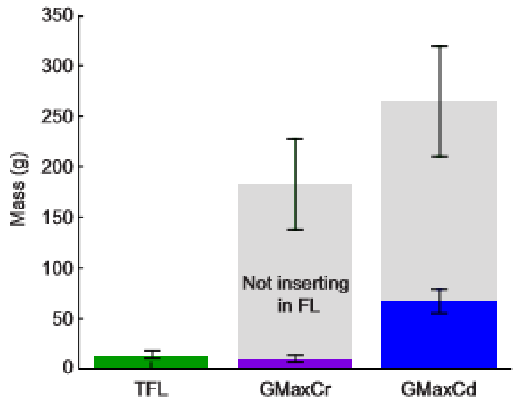

Fig. 3. Mass of the chimpanzee TFL, GMaxCr and GMaxCd muscles inserting on the FL versus the femur. All of the TFL muscle mass inserts in the chimp FL, but only 5% of the GMaxCr mass and 25% of the GMaxCd mass inserts in the FL.

Table 1. Muscle architecture of the chimpanzee tensor fascia lata, cranial gluteus maximus and caudal gluteus maximus muscles

Muscle	Mass (g)	Fascicle length (cm)	Pennation angle (deg)	PCSA (cm^2)*
TFL	14.0±3.8	121.8±1.5	1.7±1.7	1.2±0.4
GMaxCr1[‡]	10.2±3.4	107.2±6.0	5.0±2.9	0.7±0.6
GMaxCr2	84.3±21.0	85.2±8.9	22.3±6.7	10.0±3.3
GMaxCr3	88.1±25.5	85.3±12.4	22.3±6.7	9.7±4.9
GMaxCd1[§]	94.2±22.4	123.0±3.8	18.3±3.3	7.8±2.0
GMaxCd2	103.3±32.1	170.0±20.0	18.3±1.7	6.5±1.7
GMaxCd3	29.4±7.8	178.7±11.3	16.7±3.3	2.0±0.2
GMaxCd4	37.5±4.2	149.0±19.7	16.7±1.7	2.7±0.3

Data are expressed as means±s.e.m. Shaded muscle regions do not insert on the FL.

*Pennation angle is not included in the PCSA calculation because our SIMM model multiplies PCSA, specific tension and pennation angle to determine the maximum isometric force of a muscle.

[‡]GMaxCr1 represents the anteriormost muscle portion, whereas GMaxCr3 the posteriormost muscle portion.

[§]GMaxCd1 represents the superiormost muscle portion, whereas GMaxCd4 the inferiormost muscle portion.

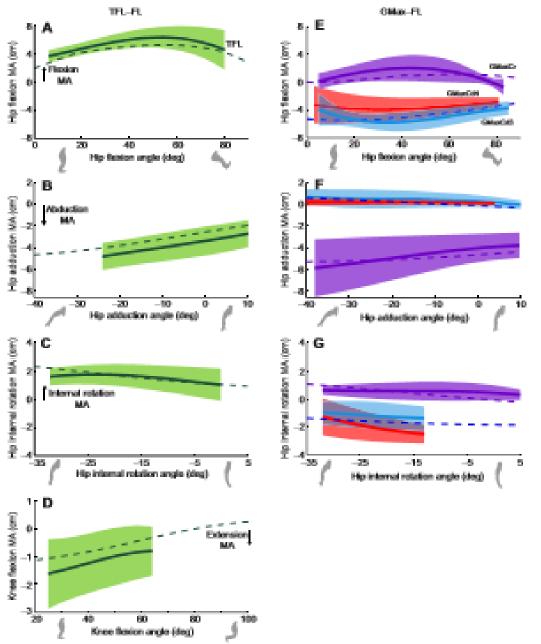

Fig. 4. Hip and knee moment arms of TFL and GMax MTUs compared with experimental data. (A) TFL has a large hip flexion moment arm (MA). (B) TFL has a large hip abduction moment arm that increases as the hip abducts (negative values of hip adduction). (C) TFL has an internal rotation moment arm that increases with external rotation. (D) TFL has a small knee extension moment arm that increases with knee extension. (E) All portions of GMaxCd–FL_{post} have large hip extension moment arms that increase with hip extension; GMaxCr–FL_{ant} has a small hip flexion moment arm. (F) All portions of GMaxCd–FL_{post} have small hip adduction moment arms, whereas GMaxCr–FL_{ant} has a large hip abduction moment arm that increases with hip abduction. (G) All portions of GMaxCd–FL_{post} have external rotation moment arms; GMaxCr–FL_{ant} has an external rotation moment arm. Solid lines and shaded regions indicate the means and s.d. of experimentally determined moment arms from four cadaveric limbs. Dashed lines show the moment arms of TFL–FL_{ant} (green), GMaxCr–FL_{ant} (purple), and the combined path of GMaxCd3,4–FL_{post} (blue) predicted by our chimp model.

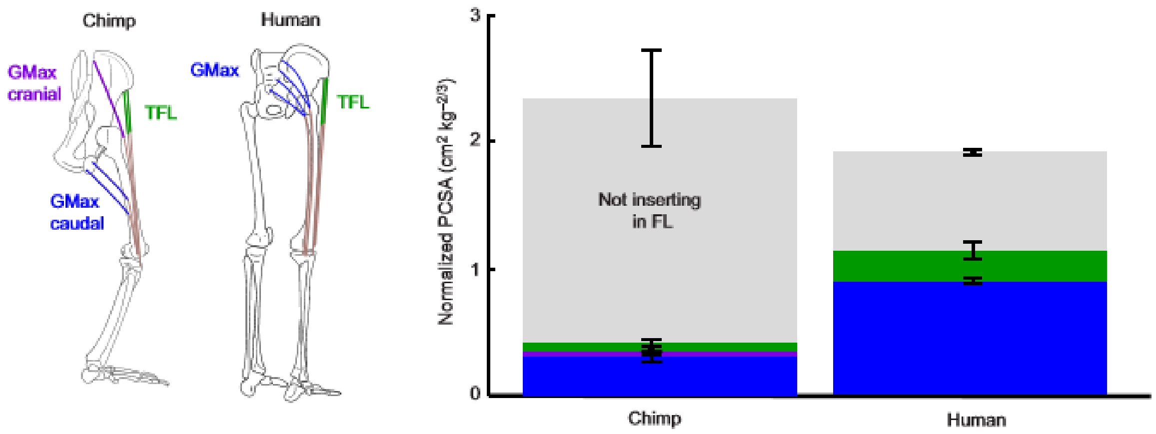

Fig. 5. The muscles inserting on the human ITB have the potential to transmit substantially larger forces than muscles inserting on the chimp FL. Normalized muscle PCSA (PCSA/body mass$^{2/3}$) for the portions of TFL (green), GMaxCr (purple) and GMaxCd (blue) that insert in the chimp FL or human ITB compared with the total normalized PCSA of the muscle regions not inserting in the FL or ITB.

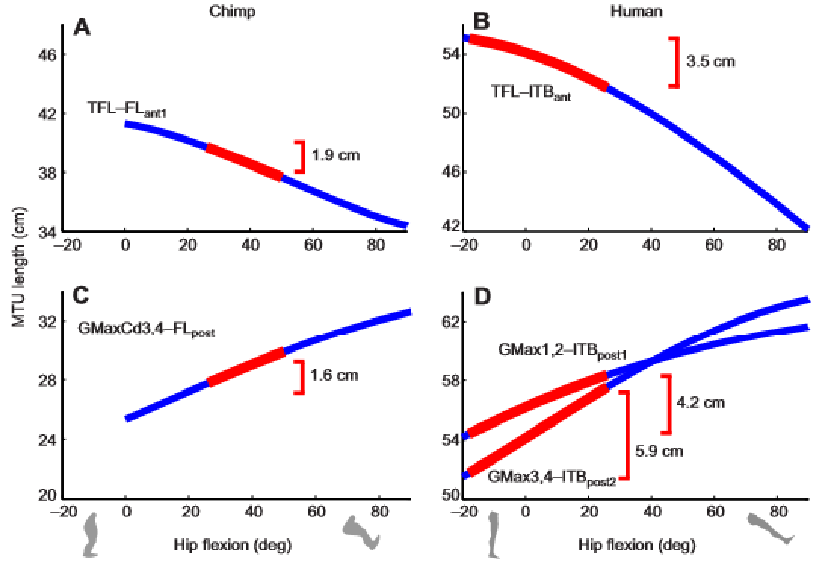

Fig. 6. MTU length as a function of hip flexion in the chimp FL and human ITB. MTU length in the anterior chimp FL (A), anterior human ITB (B) and the posterior chimp FL (C) and posterior human ITB (D). The thickened red regions show the range of hip flexion/extension angles during bipedal walking, which is lower in chimps compared with humans. The brackets indicate the change in MTU length occurring during bipedal walking due to changes in hip flexion/extension. The slope of the curve is equivalent to the moment arm of the MTU.

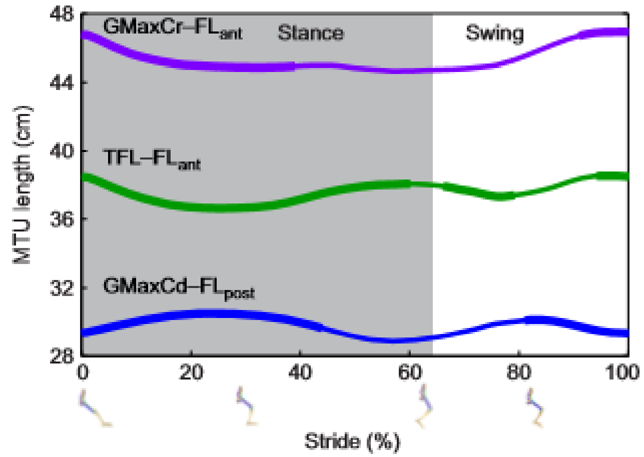

Fig. 7. MTU length during a stride of bipedal walking in the chimp. MTU length in TFL–FL$_{ant}$, GMaxCr–FL$_{ant}$ and GMaxCd–FL$_{post}$. Thickened portions of each curve denote periods in the stride when the muscles are active as recorded in Stern and Susman (1981). EMG recordings from chimps confirm that TFL, GMaxCr and GMaxCd are active when the MTU is stretched or at its

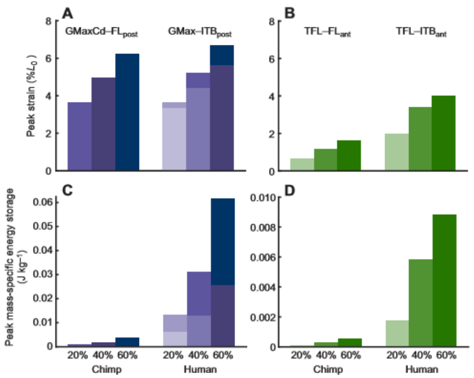

Fig. 8. Peak energy storage is greater in the human ITB than in the chimp FL. (A) Peak posterior chimp FL and human ITB strain during bipedal walking when the muscles are activated at 20, 40 and 60% of maximum. (B) Peak anterior chimp FL and human ITB strain when the muscles are activated at 20, 40 and 60% of maximum. (C) Peak elastic energy storage in the posterior chimp FL and human ITB during bipedal walking when the muscles are activated at 20, 40 and 60% of maximum. (D) Peak elastic energy storage in the anterior chimp FL and human ITB during bipedal walking when the muscles are activated at 20, 40 and 60% of maximum. For the posterior human ITB, the GMax1,2–ITB$_{post}$ is shown in light purple, whereas the GMax3,4–ITB$_{post}$ is shown in dark purple.

analysis provides little evidence that the human ITB is specialized to transmit forces in the frontal plane to stabilize the pelvis and support the torso against gravity during walking.

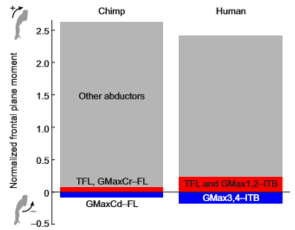

Fig. 9. The maximum frontal plane moment transmitted to the chimp FL and human ITB relative to the maximum frontal plane moment transmitted by the other hip abductors to the femur. Frontal plane moments (transmitted when muscle activation is 100%) are normalized by body mass and hemi-pelvis width. In both the human and chimp, the TFL and anterior GMax MTUs (red) have the capacity to generate small frontal plane moments about the hip that help support the pelvis and torso. By contrast, GMax3,4–ITB$_{post}$ in the human (blue) and GMaxCd–FL$_{post}$ in the chimp (blue), both generate an opposing moment at the hip that pulls the pelvis inferiorly. Other hip abductors included in the chimp and human models are gluteus medius, gluteus minimus, piriformis, sartorius, rectus femoris; the chimp model also includes iliacus and the human model includes gemelli. The portions of the human GMax1,2 and chimp GMaxCr inserting in the femur were also included in this group.

DISCUSSION

This study tested whether the human ITB is specialized for elastic energy storage relative to the chimp FL. We conducted detailed anatomical experiments on the largest sample of chimp lower extremities to date, and we analyzed musculoskeletal models of both humans and chimps to test four hypotheses.

First, we asked whether the muscles inserting on the human ITB have a greater force-generating capacity than the muscles inserting on the chimp FL, after accounting for body mass (H1). We found that, in total, the force-generating capacity of the muscles inserting on the ITB is three times greater than the force-generating capacity of the muscles inserting on the FL, suggesting substantially greater forces are transmitted via the ITB compared with the FL. This greater capacity for force primarily stems from the fact that only about 10% of the chimp TFL, GMaxCr and GMaxCd mass inserts in the FL, whereas nearly 60% of the human TFL and GMax mass inserts in the ITB.

Second, we hypothesized that the human ITB undergoes greater strains than the chimp FL during typical bipedal walking kinematics (H2). We found that the greater MTU length changes and greater mass-specific force-generating capacity of the human TFL result in greater peak strains in the human anterior ITB than the chimp anterior FL. The anterior ITB in humans stretches more than the anterior FL in chimps because humans walk with greater hip flexion/extension excursion than chimps (O'Neill et al., 2015). Contrary to our hypothesis, peak strains in the posterior ITB and posterior FL are similar in our models. However, consistent with our third hypothesis that the human ITB has a substantially greater potential to store elastic energy, per unit body mass, than the chimp FL during bipedal walking (H3), the larger forces transmitted to the posterior ITB result in substantially greater energy storage. Thus, differences in both anatomy and locomotor mechanics between chimpanzees and humans determine the human ITB's greater elastic energy storage capacity compared with the chimp FL.

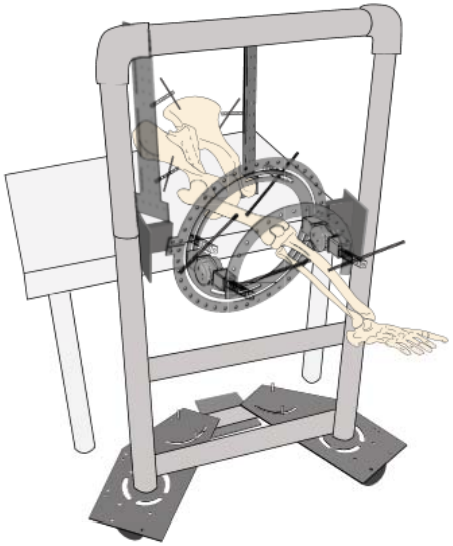

Fig. 10. Chimpanzee lower limbs were mounted in a frame for measuring muscle moment arms. The custom-made frame comprises a fixed platform for aligning and securing the pelvis, an adjustable cart for moving the femur through a range of hip flex/extension and abduction/adduction angles, and a set of concentric rings for rotating the femur about its mechanical axis, following Arnold et al. (2000).

Representation of MTU paths in the musculoskeletal model

We modified paths of the TFL–FL and GMax–FL MTUs in the musculoskeletal model reported by O'Neill et al. (2013) to match our digitized muscle attachments, regional paths and moment arm data (Fig. 11). Using SIMM, we created two paths for TFL, one path for GMaxCr, and two paths for GMaxCd. MTUs were represented as line segments spanning from origin to insertion and were constrained by 'via' points (points through which a muscle is constrained to act) and wrap objects to simulate underlying structures and more accurately estimate changes in length with changes in joint angle (supplementary material Fig. S1). Via points and wrapping surfaces were iteratively adjusted so that the paths resembled the paths digitized during the experiments and the model's moment arms

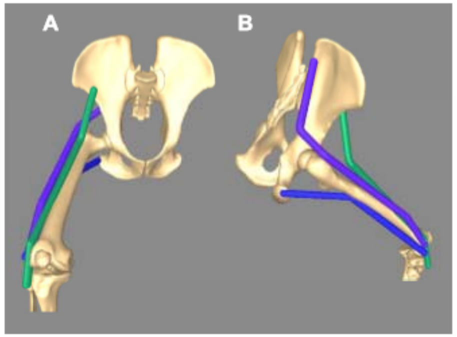

Fig. 11. The chimp lower extremity model modified from O'Neill et al. (2013). (A) Anterolateral view of the chimp lower extremity model showing TFL–FL_{ant} (green), GMaxCr–FL_{ant} (purple) and GMaxCd–FL_{post} (blue). (B) Posterolateral view of the chimp model showing the FL MTU paths.

Published in final edited form as:
Neuroimage. 2015 March ; 108: 124–137. doi:10.1016/j.neuroimage.2014.12.039.

Virtual dissection and comparative connectivity of the superior longitudinal fasciculus in chimpanzees and humans

Erin E. Hecht[1,2], David A. Gutman[3], Bruce A. Bradley[4], Todd M. Preuss[5], and Dietrich Stout[6]

[1]Department of Anthropology Emory University

[2]Department of Psychology Center for Behavioral Neuroscience Georgia State University

[3]Department of Biomedical Informatics Emory University School of Medicine 36 Eagle Row, PA Building, 5th Floor South Atlanta, GA 30322 dgutman@emory.edu

[4]Department of Archaeology University of Exeter Laver Building, North Park Road Exeter EX4 4QE, United Kingdom B.A.Bradley@exeter.ac.uk

[5]Yerkes National Primate Research Center Div. Neuropharmacology & Neurologic Diseases & Center for Translational Social Neuroscience Emory University 954 Gatewood Rd. Atlanta, GA 30329 tpreuss@emory.edu

[6]Department of Anthropology Emory University 1557 Dickey Drive, Rm 114 Atlanta, GA 30322 dwstout@emory.edu

for the evolution of fronto-parietal functions including spatial attention to observed actions, socia learning, and tool use, and are in line with previous research suggesting a unique role for the righ anterior inferior frontal gyrus in the evolution of human fronto-parietal network architecture.

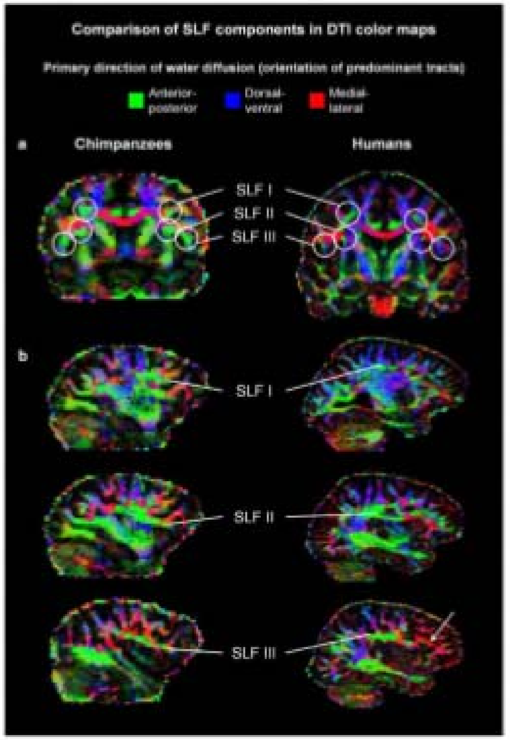

Figure 1. Portions of SLF I, II, and III visible in the DTI color map before tractography
(a) Coronal slice in representative chimpanzee and human subjects showing all 3 tracts. (b) Parasagittal slices showing each tract. Note the medial-lateral crossing fibers in the inferior frontal sections of SLF II and especially SLF III in humans (white arrow).

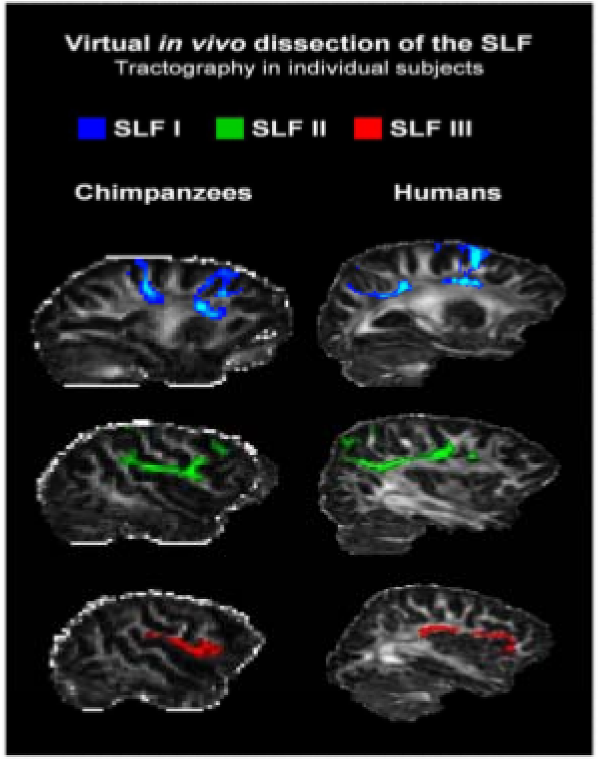

Figure 2. SLF tracts in individual subjects

Parasagittal slices in representative chimpanzee and human subjects showing SLF I (top, blue), SLF II (middle, green), and SLF III (bottom, red).

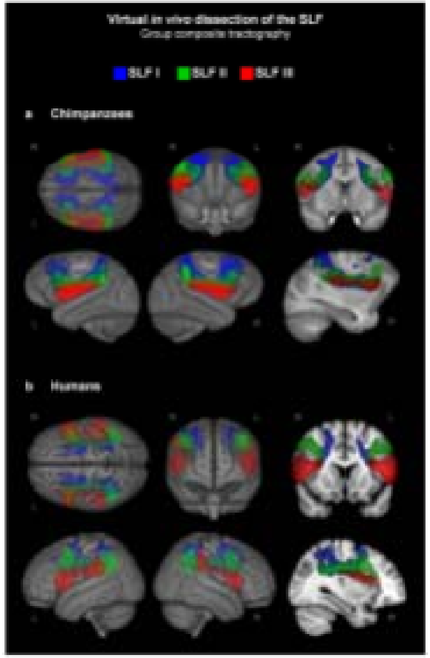

Figure 3. Group composite images of SLF tracts

Results in individual subjects were thresholded at .1% of the waytotal, binarized, registered to template space, and summed, so that in these composite images, intensity corresponds to the number of subjects with above-threshold connectivity at that voxel. Group composite tracts were thresholded to show only above-threshold connectivity common to at least 50% of subjects. (a) Chimpanzees. (b) Humans. The right-most images in each row are 2D slices; the rest are 3D renderings of white matter tracts onto the brain surface.

[redacted]

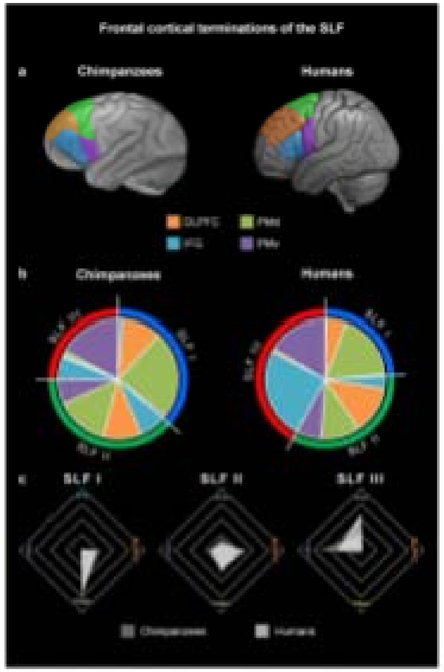

Figure 4. Quantification of SLF tracts

(a) Regions of interest used to quantify frontal cortical connectivity. (b) Blue, green, and red bands represent proportion of total SLF frontal connectivity from SLF I, II, and III, respectively. Pie charts show connectivity of each frontal region relative to the entire SLF (percent of the entire SLF's total frontal gray matter terminations). (c) Radar plots show connectivity of each frontal region relative to a particular branch of the SLF (percent of that particular tract's total frontal gray matter terminations). IFG, inferior frontal gyrus. DLPFC, dorsolateral prefrontal cortex. PMd, dorsal premotor cortex. PMv, ventral premotor cortex. Anatomical boundaries for each ROI are listed in Table 1. Panel a is modified with permission from Hecht et al., J Neurosci 2013 33(35):14117-34.

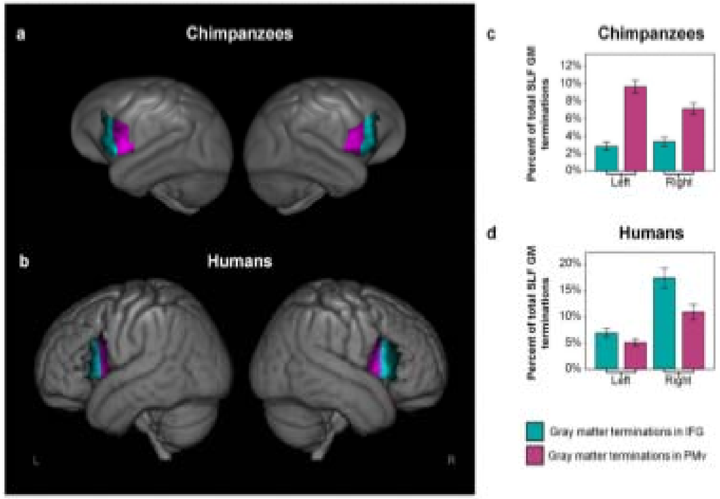

Figure 6. Lateralization of the frontal terminations of SLF III

(a) In chimpanzees, the gray matter terminations of SLF III occur mainly in the ventral precentral gyrus in both hemispheres. (b) In humans, the anterior termination of the left SLF III is occurs largely in the pars opercularis of the inferior frontal gyrus, while the right SLF III terminates more anteriorly, in the pars triangularis and pars orbitalis. (c) In chimpanzees, PMv connections outweigh IFG connections in both hemispheres. (d) In humans, IFG connections are significantly greater than PMv connections in both hemispheres.

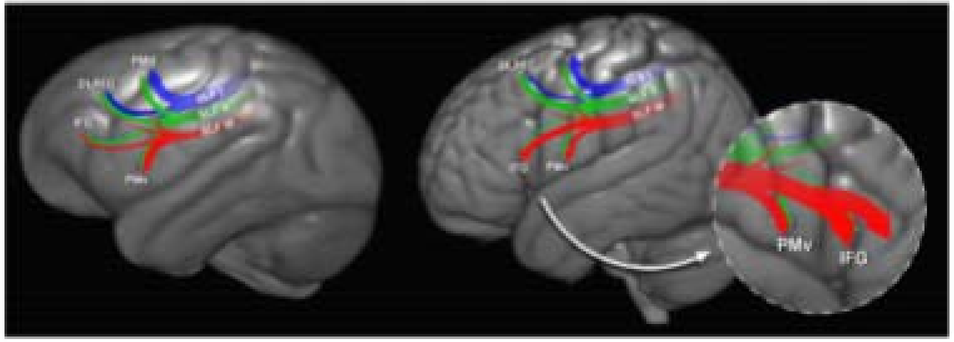

Figure 7. Diagram of the frontal connectivity of the superior longitudinal fasciculus in chimpanzees and humans

(a) Chimpanzees. (b) Humans. The width of the main body of each tract is proportional to the volume of that tract's white matter relative to the total white matter of the SLF. The widths of the cortical terminations of each tract are proportional to the volume of gray matter connectivity of that tract within that region relative to the total gray matter connectivity of the SLF. All measurements represent average measurements across both hemispheres, except for the inferior frontal terminations of SLF III, which are depicted separately for the left and right hemisphere. The pattern of SLF I connectivity was similar across species. In SLF II, humans showed more DLPFC connectivity and less IFG connectivity. In SLF III, humans showed more IFG connectivity and less PMd connectivity. Humans also showed a lateralization effect in the inferior frontal terminations of SLF III which was not apparent in chimpanzees, namely, an extension of right SLF III into the more anterior aspects of the inferior frontal gyrus.

Table 1

Anatomical definitions of homologous human and chimpanzee regions of interest for quantifying frontal SLF terminations. Chimpanzee ROIs were drawn by hand based on previous anatomical research (Brodmann 1909, Economo and Parker 1929, Bailey 1948, Von Bonin 1948, Bailey and Von Bonin 1950, Schenker, Hopkins et al. 2010). Human ROIs were created using the Julich probabilistic cytoarchitectonic atlas (Eickhoff, Paus et al. 2007) and the Harvard/Oxford probabilistic structural atlas (Desikan, Segonne et al. 2006). Reproduced with permission and modified from Hecht et al., J Neurosci 2013 33(35):14117-34.

Region of interest	Chimpanzees		Humans	
	Anatomical description	Cyto-architectonic region(s)	Anatomical description	Cyto-architectonic region(s)
Dorsal premotor cortex (PMd)	At its dorsal aspect, it extends anteriorly to an imaginary line drawn from the tip of the inferior pre-central sulcus at a 90 degree angle with the lateral sulcus. The inferior part of the ROI is bordered anteriorly at the inferior frontal sulcus, curving down and back to meet the PMv ROI. The border between PMd and PMv is an imaginary line drawn parallel to the lateral sulcus at the dorsal tip of the fronto-occipital sulcus so that the superior borders of PMv and Broca's area are continuous.	FB (BA 6), FC (BA 8)	Its posterior border is a vertical line from the lateral sulcus to the superior tip of the superior pre-central sulcus. Its anterior border is a 45 degree line from the antero-superior edge of the PMv ROI. The border between PMd and PMv is the gyrus that splits the superior and inferior precentral sulci.	BA 6, BA 8
Ventral premotor cortex (PMv)	Bordered posteriorly by the M1/S1 ROI, superiorly as described above, and anteriorly by the inferior precentral sulcus.	FBA (BA 6)	Its anterior border is the inferior precentral sulcus. Its posterior border is a vertical line from the lateral sulcus to the superior tip of superior pre-central sulcus (M1). Its superior border is the gyrus that splits the inferior and superior precentral gyri.	BA 6
Dorso-lateral prefrontal cortex (DLPFC)	Bordered dorsally by the interhemispheric fissure, posteriorly by the PMd ROI, inferiorly by the Broca's area ROI, and anteriorly by an imaginary line which is an extension of the orbital sulcus drawn past the tip of the middle frontal sulcus.	FDm (BA 9), Fddelta (BA 46)	Its inferior border is the inferior frontal sulcus. Its anterior border is a 45 degree line drawn from tip of anterior horizontal ramus (the sulcus that borders the anterior edge of Broca's area).	BA 9, BA 46
Inferior frontal gyrus (IFG)	Includes the pars opercularis and pars triangularis of the inferior frontal gyrus. Bordered posteriorly by the inferior precentral sulcus, anteriorly by the small sulcus that extends anteriorly from the fronto-orbital sulcus, and superiorly by the inferior frontal sulcus.	FCBm (BA 44), FDp (BA 45)	Same.	BA 44, BA 45

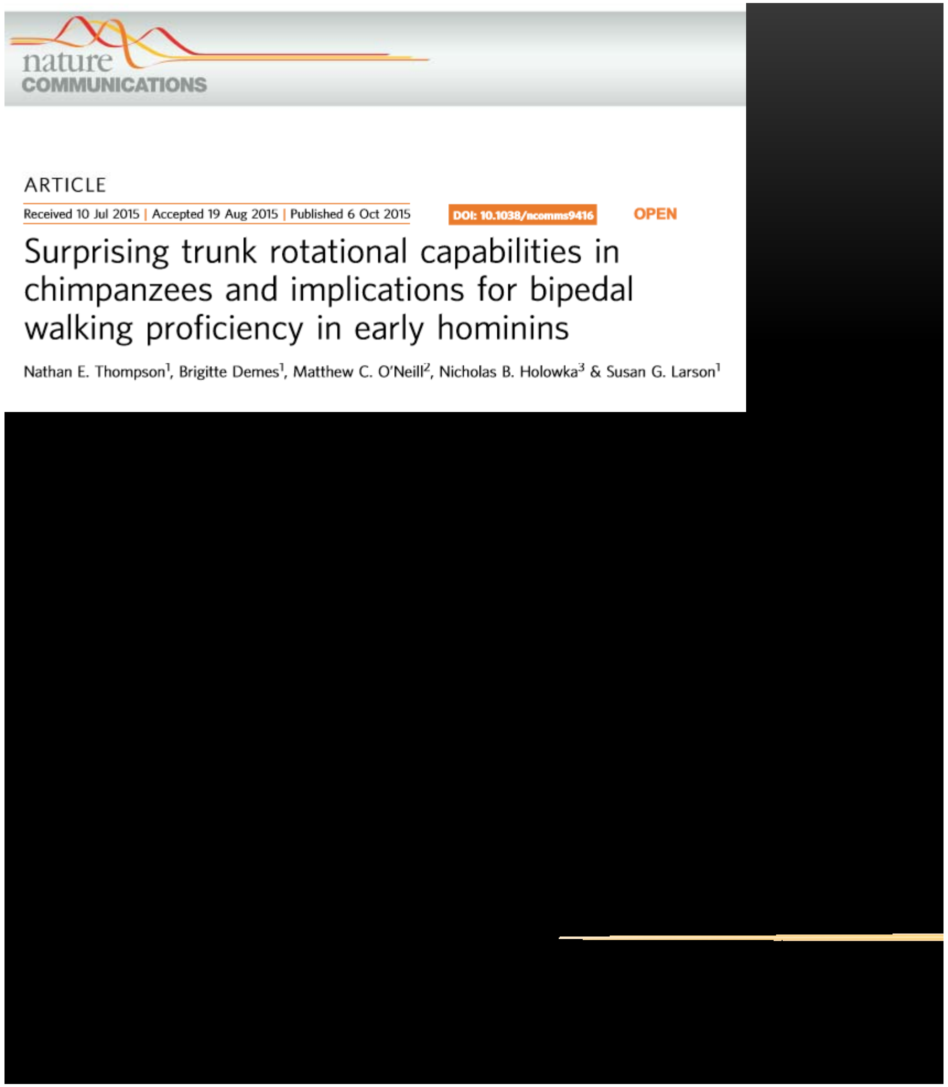

nature COMMUNICATIONS

ARTICLE

Received 10 Jul 2015 | Accepted 19 Aug 2015 | Published 6 Oct 2015 DOI: 10.1038/ncomms9416 OPEN

Surprising trunk rotational capabilities in chimpanzees and implications for bipedal walking proficiency in early hominins

Nathan E. Thompson[1], Brigitte Demes[1], Matthew C. O'Neill[2], Nicholas B. Holowka[3] & Susan G. Larson[1]

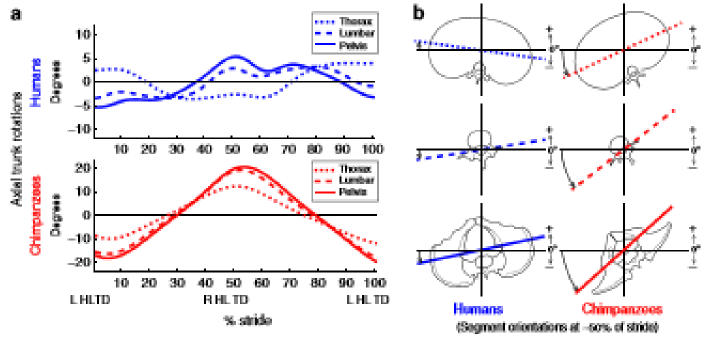

Figure 1 | Mean angular motion of all segments for humans and chimpanzees over a stride. (a) Rotations are relative to a global coordinate system. Note the difference in *y* axis scale between species. LHLTD and RHLTD represent left and right hind limb touchdowns, respectively. **(b)** Angular motions near 50% of stride for humans and chimpanzees with segment motion represented by transverse lines (rotations exaggerated to enhance clarity). The chimpanzee thorax remains in phase with the pelvis, in contrast to the out-of-phase relationship in humans.

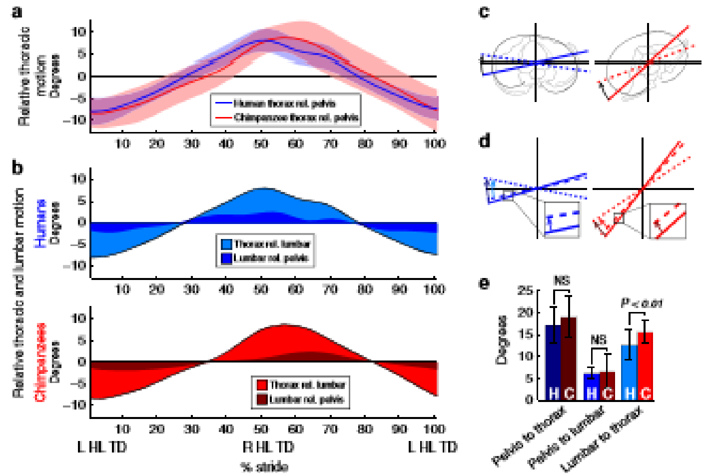

Figure 2 | Relative motion of segments to one another in humans and chimpanzees. (a) Motion of the thorax relative to the pelvis over a stride (mean ± s.d.). **(b)** Relative pelvis-to-thorax motion partitioned by the contributions of the lumbar and thoracic segments. **(c,d)** Angular motions near 50% of stride for humans and chimpanzees with segment motion represented by transverse lines (rotations exaggerated to enhance clarity). **(e)** Total range of relative pelvis-to-thorax, pelvis-to-lumbar and lumbar-to-thorax motion over a stride (mean ± s.d.). H and C represent humans and chimpanzees, respectively; NS represents non-significance using a Wilcoxon rank-sum test at the $P = 0.05$ level.

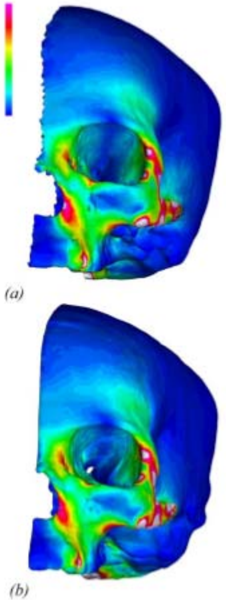

(a)

(b)

Figure S2. Von Mises stress distributions in Finite Element Models (FEMs) of half crania of (a) H. sapiens and (b) a merged model comprising ~ 15% H. sapiens mesh (external facial region) and 85% a mesh of P. troglodytes deformed to fit the original geometry of H. sapiens

PROCEEDINGS OF THE ROYAL SOCIETY B

Proc. R. Soc. B (2010) **277**, 3579–3586
doi:10.1098/rspb.2010.0509
Published online 23 June 2010

The craniomandibular mechanics of being human

Stephen Wroe[1,*], Toni L. Ferrara[1], Colin R. McHenry[1,2], Darren Curnoe[1] and Uphar Chamoli[1]

[1]*Computational Biomechanics Research Group, Evolution and Ecology Research Centre, School of Biological, Earth and Environmental Sciences, University of New South Wales, Sydney, NSW 2052, Australia*
[2]*School of Engineering, University of Newcastle, NSW 2308, Australia*

Diminished bite force has been considered a defining feature of modern *Homo sapiens*, an interpretation inferred from the application of two-dimensional lever mechanics and the relative gracility of the human masticatory musculature and skull. This conclusion has various implications with regard to the evolution of human feeding behaviour. However, human dental anatomy suggests a capacity to withstand high loads and two-dimensional lever models greatly simplify muscle architecture, yielding less accurate results than three-dimensional modelling using multiple lines of action. Here, to our knowledge, in the most comprehensive three-dimensional finite element analysis performed to date for any taxon, we ask whether the traditional view that the bite of *H. sapiens* is weak and the skull too gracile to sustain high bite forces is supported. We further introduce a new method for reconstructing incomplete fossil material. Our findings show that the human masticatory apparatus is highly efficient, capable of producing a relatively powerful bite using low muscle forces. Thus, relative to other members of the superfamily Hominoidea, humans can achieve relatively high bite forces, while overall stresses are reduced. Our findings resolve apparently discordant lines of evidence, i.e. the presence of teeth well adapted to sustain high loads within a lightweight cranium and mandible.

Keywords: form and function; Hominoidea; fossil

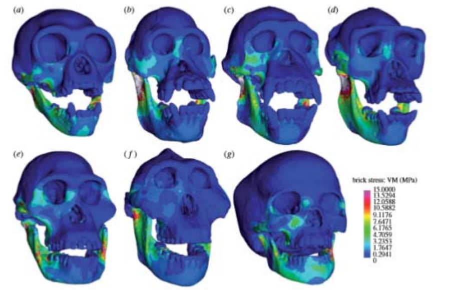

Figure 1. Visual plots of von Mises (VM) stress distributions in finite element models scaled to a uniform surface area and bite force simulating unilateral bites at the second molar: (a) *Hylobates lar*; (b) *Pongo pygmaeus*; (c) *Pan troglodytes*; (d) *Gorilla gorilla*; (e) *Australopithecus africanus*; (f) *Paranthropus boisei*; (g) *Homo sapiens*. Dark blue regions show no or minimal stress with stress increasing to 15 MPa in pink regions. Highest stresses are in white regions, i.e. greater than 15 MPa.

anthropoid primates (Wall 1999). We conclude that although humans are well adapted to produce high peak forces with the jaw moving in rotation, they may not be as well adapted to produce and maintain high bite forces with the jaw moving in translation. Thus, *Homo sapiens* may be comparable to other hominids in possessing an ability to access some relatively hard foods

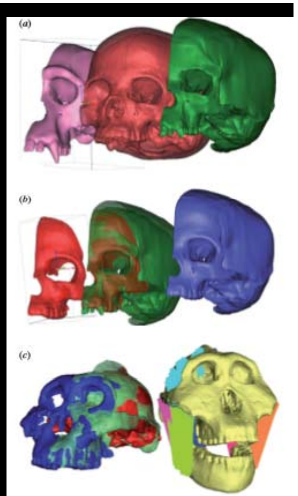

Figure 2. Reconstruction. (a) To test protocols for reconstructing missing data in fossil skulls a left-side half cranial mesh of *P. troglodytes* (pink) was warped to fit the left side of a cranial mesh of a *H. sapiens* (red) to produce a deformed *Pan* mesh (green). (b) The left facial region of the original *H. sapiens* mesh was isolated and internal geometry removed (red). This was merged with the deformed *Pan* to produce a new '*H. sapiens*' mesh (blue) in which approximately 85% of original *H. sapiens* geometry was replaced by the deformed *Pan*. Performance of a finite element model (FEM) based on this reconstructed half cranial mesh was compared with that of a half cranial FEM generated from the original *H. sapiens* data. Under equivalent loadings, stress distributions were almost identical in both FEMs (see electronic supplementary material). (c) Meshes of *P. boisei* facial skeleton (blue) and posterior cranium (red) superimposed on half-cranial mesh warped from an STL of *P. troglodytes* to fit fossil material (green); and FEM of *P. boisei* with muscles modelled as pre-tensioned truss elements.

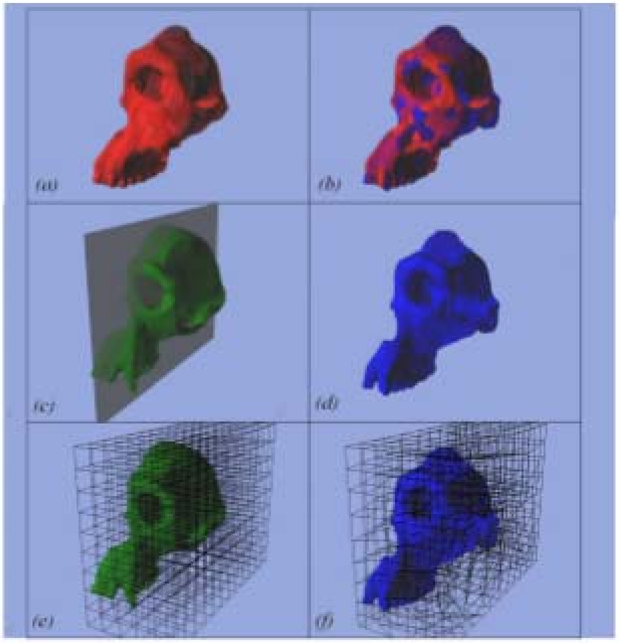

Figure S1. Reconstruction of fossil material - meshes of the left cranium (and see Materials and Methods). (*a*) ***P. boisei*** (cast and fossil combined). (*b*) Undeformed ***Pan***. (*c*) ***Pan*** skull and 3D grid prior to deformation. (*d*) ***P. boisei*** mesh with deformed Pan mesh (blue) superimposed. (*e*) Deformed ***Pan*** mesh. (*f*) ***Pan*** mesh and 3D grid after at end of deformation process.

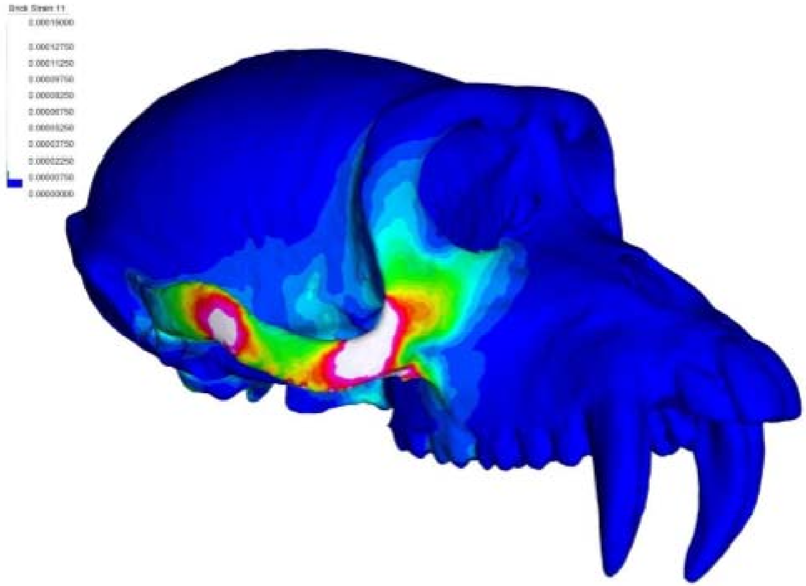

Figure S4. Surface plot of maximum principal strain distribution in a Finite Element Model (FEM) of *Macaca fascicularis* (MAC-17) as determined using protocols applied to the generation of hominid FEMs used in the present study but with constraints and loadings as applied in a previous analysis (Kupczik et al. 2007). Results using our methods correspond well with experimentally derived strains (Kupczik et al. 2007). Note that white regions show highest strain.

Table S2. Cross sectional areas, muscle forces and pretensions for muscle trusses

Species	Temporalis	Masseter	Medial pterygoid	Ref(Demes & Creel 1988)
Gorilla gorilla	17.9; 625.8; 20.9	15.3; 536.9; 16.3	11.0; 383.6; 22.6	13.5 +/- 2.0; n=3
Pan troglodytes	15.0; 525.0; 17.5	13.8; 483.4; 14.6	9.5; 332.9; 19.6	10.3 +/- 0.9; n=4
Pongo pygmaeus	10.3; 360.5; 12.0	10.3; 361.9; 11.0	6.8; 238.4; 14.0	11.7 +/- 2.8; n=3
Hylobates lar	3.2; 112.0; 3.7	2.1; 73.5; 2.2	1.8; 61.3; 3.6	2.9 +/- 0.1; n=3
Homo sapiens	8.7; 303.5; 10.1	9.5; 333.9; 10.1	7.0; 245.0;14.4	6.3 +/- 0.4; n=2
Australopithecus africanus (Sts 5)	11.0; 383.3; 12.8	7.0; 243.3; 7.4	7.0; 241.9; 14.2	9.7
Paranthropus boisei (OH 5)	19.9; 695.1; 23.2	27.7; 970.9;29.4	15.7; 549.2; 32.3	20.6

Numbers displayed for the temporalis, masseter, and medial pterygoid indicate cross sectional area (CSA; cm^2); muscle force (Newtons; N); and truss pretension (N) respectively. The same number of pre-tensioned trusses representing major muscle groups was applied to each model: temporalis (30); masseter profundus (14); masseter superfiscialis (19); medial pterygoid (17).

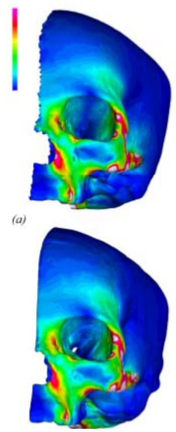

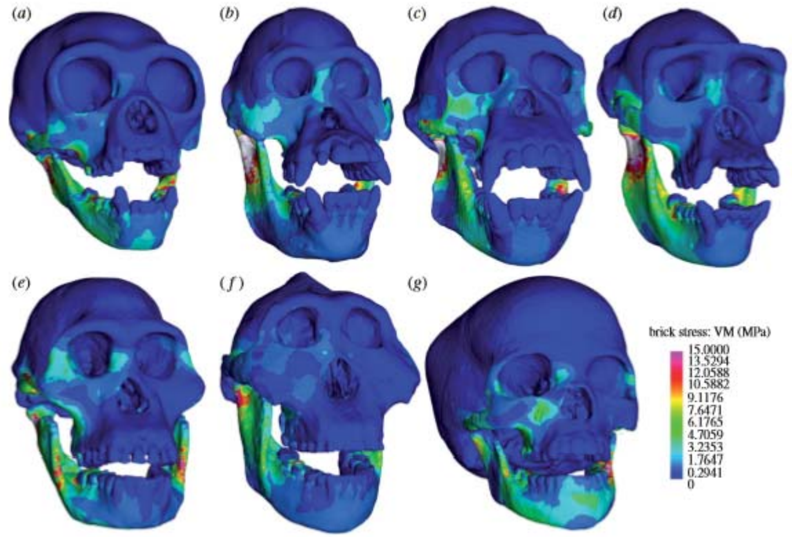

Figure 1. Visual plots of von Mises (VM) stress distributions in finite element models scaled to a uniform surface area and bite force simulating unilateral bites at the second molar: (*a*) *Hylobates lar*; (*b*) *Pongo pygmaeus*; (*c*) *Pan troglodytes*; (*d*) *Gorilla gorilla*; (*e*) *Australopithecus africanus*; (*f*) *Paranthropus boisei*; (*g*) *Homo sapiens*. Dark blue regions show no or minimal stress with stress increasing to 15 MPa in pink regions. Highest stresses are in white regions, i.e. greater than 15 MPa.

Brackets Self-ligating We Pass Tecnica Roth

WePass™

Mandibolare

Mascellare

TECNICA ROTH

Il kit comprende i tubi per I e II molare

Torque			-7°	-7°	-2°	+8°	+12°	+12°	+8°	-2°	-7°	-7°
Tip			0°	0°	+11°	+9°	+5°	+5°	+9°	+11°	0°	0°
in/out mm			0,7	0.7	0.7	1.1	0.8	0.8	1.1	0.7	0.7	0.7
width mm			2.8	2.8	2.8	2.75	3.1	3.1	2.7	2.8	2.8	2.8
REF	18°	Senza gancio	BR821-10144	BR811-10144	BR811-10134	BR811-10124	BR811-10114	BR811-10214	BR811-10224	BR811-10234	BR811-10244	BR811-10244
		Con gancio	BR821-11144	BR811-11144	BR811-11134	-	-	-	-	BR811-11234	BR811-11244	BR811-11244
	22	Senza gancio	BR822-10144	BR812-10144	BR812-10134	BR812-10124	BR812-10114	BR812-10214	BR812-10224	BR812-10234	BR812-10244	BR812-10244
		Con gancio	BR812-11144	BR812-11144	BR812-11134	-	-	-	-	BR812-11234	BR812-11244	BR812-11244
Confezione			2	2	2	2	2	2	2	2	2	2

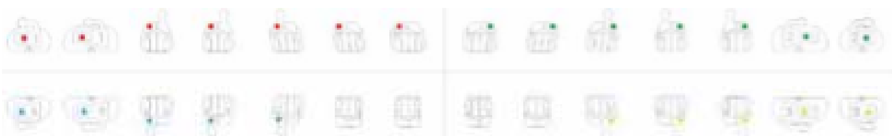

Torque			-22°	-17°	-11°	-1°	-1°	-1°	-1°	-11°	-17°	-22°
Tip			0°	0°	+5°	0°	0°	0°	0°	+5°	0°	0°
in/out mm			0.6	0.6	0.7	1.1	1.1	1.1	1.1	0.7	0.6	0.6
width mm			2.8	2.8	2.8	2.75	2.75	2.75	2.75	2.8	2.8	2.8
REF	18°	Senza gancio	BR821-10454	BR811-10444	BR811-10434	BR811-10314	BR811-10314	BR811-10314	BR811-10314	BR811-10334	BR811-10344	BR811-10354
		Con gancio	BR821-11454	BR811-11444	BR811-11434	-	-	-	-	BR811-11334	BR811-11344	BR811-11354
	22	Senza gancio	BR822-10454	BR812-10444	BR812-10434	BR812-10314	BR812-10314	BR812-10314	BR812-10314	BR812-10334	BR812-10344	BR812-10354
		Con gancio	BR812-11454	BR812-11444	BR812-11434	-	-	-	-	BR812-11334	BR812-11344	BR812-11354
Confezione			2	2	2	2	2	2	2	2	2	2

SLOT	Contenuto	Conf.	3° con gancio	3°/ 4° /5° con gancio
18	1 Kit	28 pcs	BR811-134	BR811-154
22	1 Kit	28 pcs	BR812-134	BR812-154

TECNICA MBT

Il kit comprende i tubi per I e II molare

Torque			-7°	-7°	-7°	+10°	+17°	+17°	+10°	-7°	-7°	-7°
Tip			0°	0°	+8°	+8°	+4°	+4°	+8°	+8°	0°	0°
in/out mm			0,8	0.8	0.8	1.15	0.9	0.9	1.15	0.8	0.8	0.8
width mm			2.8	2.8	2.8	2.75	3.0	3.0	2.75	2.8	2.8	2.8
REF	18°	Senza gancio	BR821-10144	BR821-10144	BR821-10134	BR821-10124	BR821-10114	BR821-10214	BR821-10224	BR821-10234	BR821-10244	BR821-10244
		Con gancio	BR821-11144	BR821-11144	BR821-11134	-	-	-	-	BR821-11234	BR821-11244	BR821-11244
	22	Senza gancio	BR822-10144	BR822-10144	BR822-10134	BR822-10124	BR822-10114	BR822-10214	BR822-10224	BR822-10234	BR822-10244	BR822-10244
		Con gancio	BR822-11144	BR822-11144	BR822-11134	-	-	-	-	BR822-11234	BR822-11244	BR822-11244
Confezione			2	2	2	2	2	2	2	2	2	2

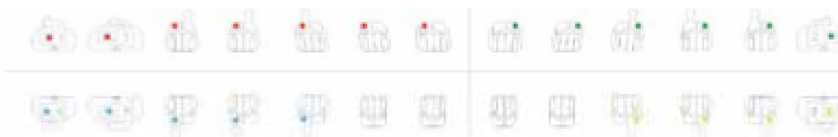

Torque			-17°	-12°	-6°	-6°	-6°	-6°	-6°	-6°	-12°	-17°
Tip			0°	0°	+3°	0°	0°	0°	0°	+3°	0°	0°
in/out mm			0.8	0.8	0.8	1.15	1.15	1.15	1.15	0.8	0.8	0.8
width mm			2.8	2.8	2.8	2.76	2.76	2.76	2.76	2.8	2.8	2.8
REF	18°	Senza gancio	BR821-10454	BR821-10444	BR821-10434	BR821-10314	BR821-10314	BR821-10314	BR821-10314	BR821-10334	BR821-10344	BR821-10354
		Con gancio	BR821-11454	BR821-11444	BR821-11434	-	-	-	-	BR821-11334	BR821-11344	BR821-11354
	22	Senza gancio	BR822-10454	BR822-10444	BR822-10434	BR822-10314	BR822-10314	BR822-10314	BR822-10314	BR822-10334	BR822-10344	BR822-10354
		Con gancio	BR822-11454	BR822-11444	BR822-11434	-	-	-	-	BR822-11334	BR822-11344	BR822-11354
Confezione			2	2	2	2	2	2	2	2	2	2

SLOT	Contenuto	Conf.	3° con gancio	3°/4°/5° con gancio
18	1 Kit	28 pcs	BR821-134	BR821-154
22	1 Kit	28 pcs	BR822-134	BR822-154

Torque differenziali

Superiore	Centrale		Laterale		Canino	
	-	+	-	+	-	+
	+5°	+22°	-3°	+13°	+0°	+7°

Inferiore	Laterale	
	-	+
	-10°	+3°

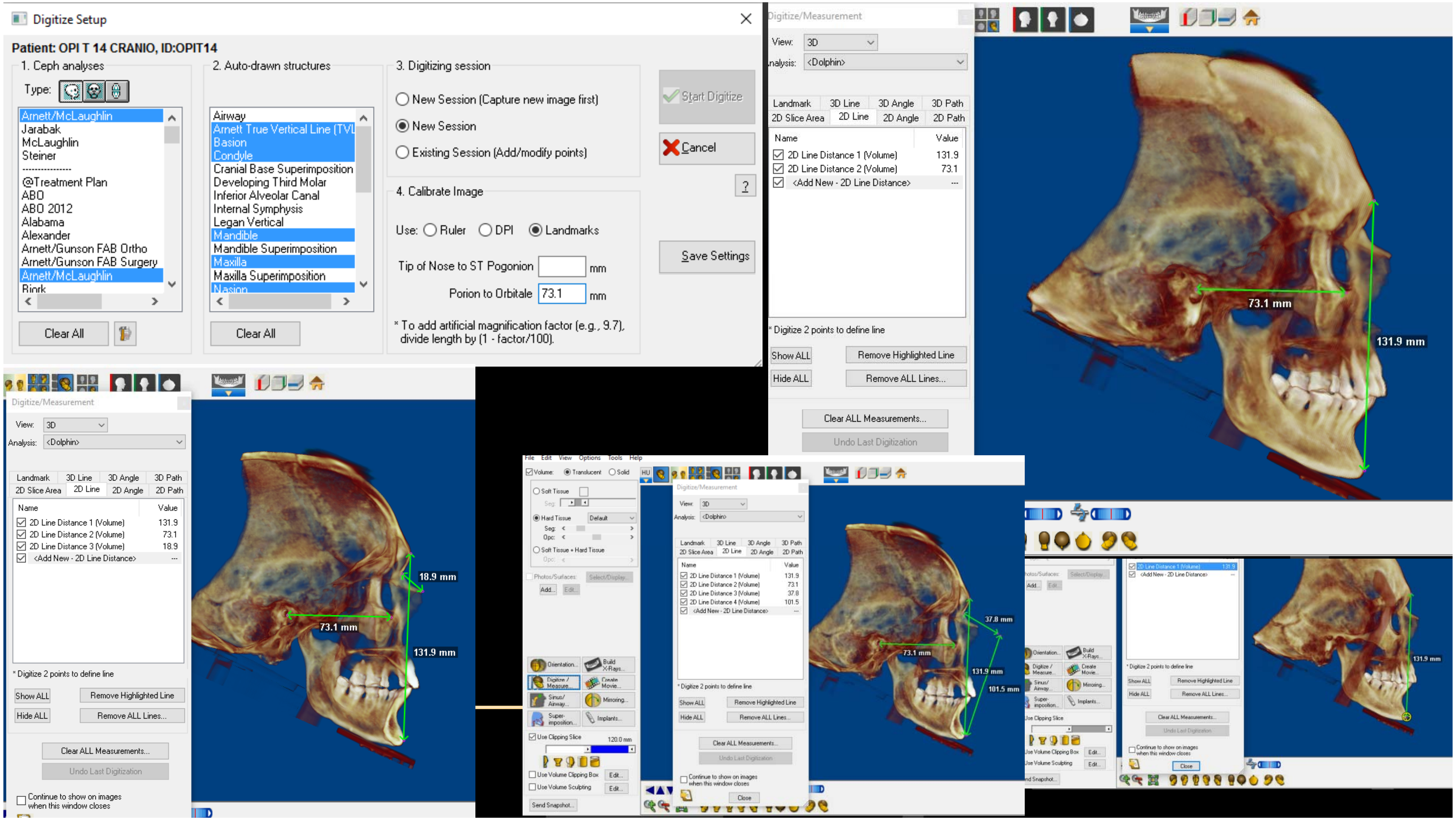
Digitize Setup
Patient: OPI T 14 CRANIO, ID:OPIT14
1. Ceph analyses
Type:
Arnett/McLaughlin
Jarabak
McLaughlin
Steiner
@Treatment Plan
ABO
ABO 2012
Alabama
Alexander
Arnett/Gunson FAB Ortho
Arnett/Gunson FAB Surgery
Arnett/McLaughlin
Bjork
Clear All
2. Auto-drawn structures
Airway
Arnett True Vertical Line (TVL
Basion
Condyle
Cranial Base Superimposition
Developing Third Molar
Inferior Alveolar Canal
Internal Symphysis
Legan Vertical
Mandible
Mandible Superimposition
Maxilla
Maxilla Superimposition
Nasion
Clear All
3. Digitizing session
New Session (Capture new image first)
New Session
Existing Session (Add/modify points)
4. Calibrate Image
Use: Ruler DPI Landmarks
Tip of Nose to ST Pogonion mm
Porion to Orbitale 73.1 mm
* To add artificial magnification factor (e.g., 9.7), divide length by (1 - factor/100).
Start Digitize
Cancel
Save Settings
Digitize/Measurement
View: 3D
Analysis: <Dolphin>
Landmark 3D Line 3D Angle 3D Path
2D Slice Area 2D Line 2D Angle 2D Path
Name Value
2D Line Distance 1 (Volume) 131.9
2D Line Distance 2 (Volume) 73.1
2D Line Distance 3 (Volume) 18.9
<Add New - 2D Line Distance>
* Digitize 2 points to define line
Show ALL
Hide ALL
Remove Highlighted Line
Remove ALL Lines...
Clear ALL Measurements...
Undo Last Digitization
Continue to show on images when this window closes
18.9 mm
73.1 mm
131.9 mm
37.8 mm
101.5 mm

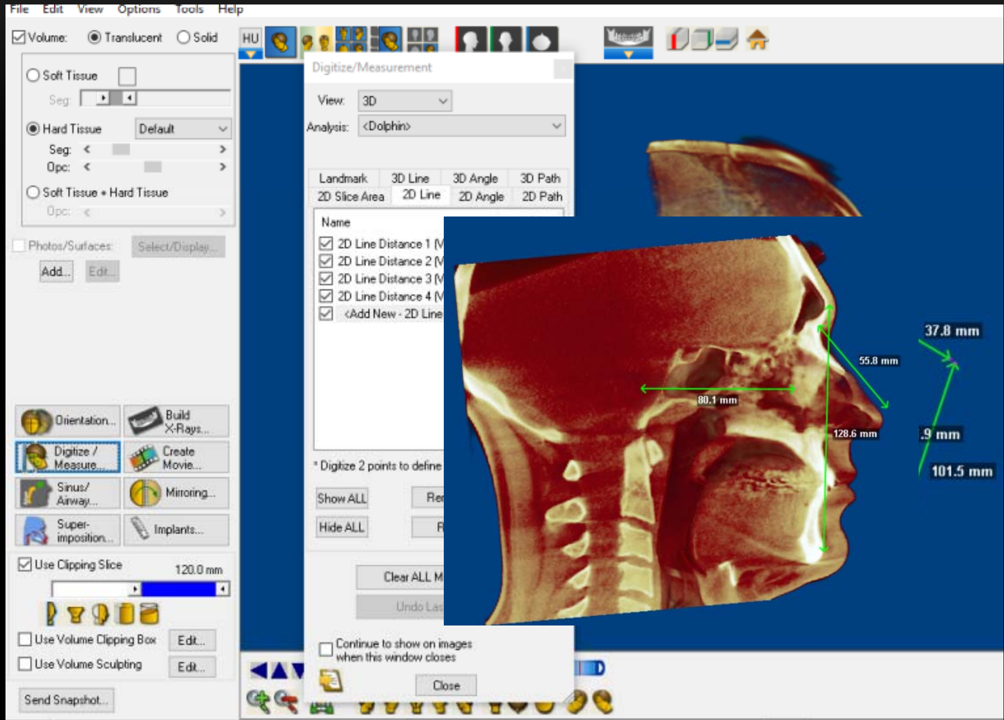
File Edit View Options Tools Help
Volume: Translucent Solid
Soft Tissue
Seg:
Hard Tissue Default
Seg:
Opc:
Soft Tissue + Hard Tissue
Opc:
Photos/Surfaces: Select/Display...
Add... Edit...
Orientation...
Build X-Rays...
Digitize / Measure...
Create Movie...
Sinus/ Airway...
Mirroring...
Super-imposition...
Implants...
Use Clipping Slice 120.0 mm
Use Volume Clipping Box Edit...
Use Volume Sculpting Edit...
Send Snapshot...
HU
Digitize/Measurement
View: 3D
Analysis: <Dolphin>
Landmark 3D Line 3D Angle 3D Path
2D Slice Area 2D Line 2D Angle 2D Path
Name
2D Line Distance 1
2D Line Distance 2
2D Line Distance 3
2D Line Distance 4
<Add New - 2D Line
* Digitize 2 points to define
Show ALL
Hide ALL
Clear ALL M
Undo Las
Continue to show on images when this window closes
Close
55.8 mm
80.1 mm
128.6 mm
37.8 mm
.9 mm
101.5 mm

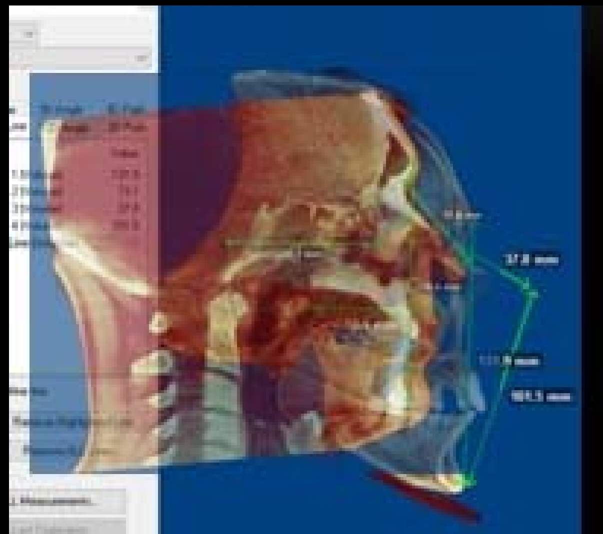

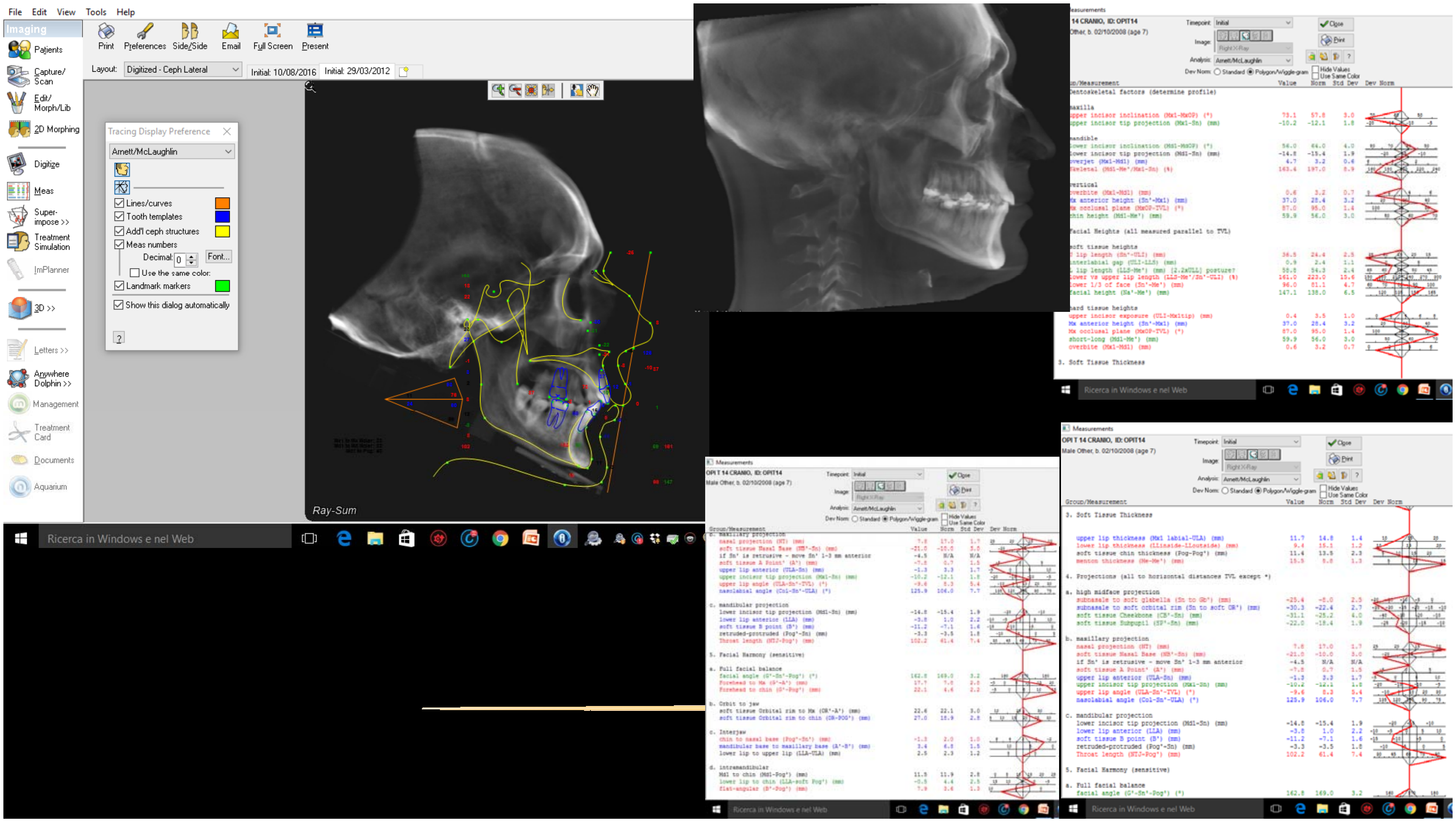
File Edit View Tools Help
Imaging
Patients
Capture/ Scan
Edit/ Morph/Lib
2D Morphing
Digitize
Meas
Super-impose >>
Treatment Simulation
ImPlanner
3D >>
Letters >>
Anywhere Dolphin >>
Management
Treatment Card
Documents
Aquarium
Print
Preferences
Side/Side
Email
Full Screen
Present
Layout: Digitized - Ceph Lateral
Initial: 10/08/2016
Initial: 29/03/2012
Tracing Display Preference
Arnett/McLaughlin
Lines/curves
Tooth templates
Add'l ceph structures
Meas numbers
Decimal: 0
Font...
Use the same color:
Landmark markers
Show this dialog automatically
Ray-Sum
Ricerca in Windows e nel Web
Measurements
OPI T 14 CRANIO, ID: OPIT14
Male Other, b. 02/10/2008 (age 7)
Timepoint: Initial
Image
Analysis: Arnett/McLaughlin
Close
Print
Hide Values
Use Same Color
Group/Measurement
Value
Norm
Std Dev
Dev Norm
3. Soft Tissue Thickness
4. Projections (all to horizontal distances TVL except *)
5. Facial Harmony (sensitive)

TECNICA ROTH

Il kit comprende i tubi per I e II molare

Torque	-7°	-7°	-2°	+8°	+12°	+12°	+8°	-2°	-7°	-7°
Tip	0°	0°	+11°	+9°	+5°	+5°	+9°	+11°	0°	0°
in/out mm	0,7	0.7	0.7	1.1	0.8	0.8	1.1	0.7	0.7	0.7
width mm	2.8	2.8	2.8	2.75	3.1	3.1	2.7	2.8	2.8	2.8
REF 18* Senza gancio	BR821-10144	BR811-10144	BR811-10134	BR811-10124	BR811-10114	BR811-10214	BR811-10224	BR811-10234	BR811-10244	BR811-10244
REF 18* Con gancio	BR821-11144	BR811-11144	BR811-11134	-	-	-	-	BR811-11234	BR811-11244	BR811-11244
REF 22 Senza gancio	BR822-10144	BR812-10144	BR812-10134	BR812-10124	BR812-10114	BR812-10214	BR812-10224	BR812-10234	BR812-10244	BR812-10244
REF 22 Con gancio	BR812-11144	BR812-11144	BR812-11134	-	-	-	-	BR812-11234	BR812-11244	BR812-11244
Confezione	2	2	2	2	2	2	2	2	2	2

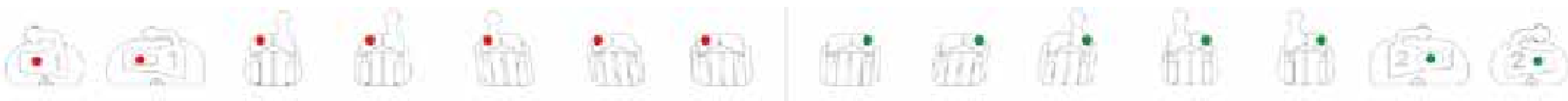

Mandibolare

Mascellare

TUBI BUCCALI COSY II per SL 1° MOLARE

System	Teeth	Torque	Offset	In/out	Width	REF	
						Non Convertible	
						.022	.018
Roth	16 (=MBT)	-14°	+10°	0.5	4	BT612-4311	BT611-4311
	26 (=MBT)	-14°	+10°	0.5	4	BT612-4312	BT611-4312
	36	-25°	+4°	0.5	4	BT612-4313	BT611-4313
	46	-25°	+4°	0.5	4	BT612-4314	BT611-4314
MBT	16	-14°	+10°	=ROTH	=ROTH	=ROTH	=ROTH
	26	-14°	+10°	=ROTH	=ROTH	=ROTH	=ROTH
	36	-20°	0°	0.5	4	BT622-4313	BT621-4313
	46	-20°	0°	0.5	4	BT622-4314	BT621-4314

TUBI BUCCALI COSY II per SL 2° MOLARE

System	Teeth	Torque	Offset	In/out	Width	REF	
						Non Convertible	
						.022	.018
Roth	16 (=MBT)	-14°	+10°	0.5	3.2	BT712-6311	BT711-6311
	26 (=MBT)	-14°	+10°	0.5	3.2	BT712-6312	BT711-6312
	36	-25°	+4°	0.5	3.2	BT712-6313	BT711-6313
	46	-25°	+4°	0.5	3.2	BT712-6314	BT711-6314
MBT	16	=ROTH	=ROTH	0.5	3.2	=ROTH	=ROTH
	26	=ROTH	=ROTH	0.5	3.2	=ROTH	=ROTH
	36	-10°	0°	0.5	3.2	BT722-6313	BT721-6313
	46	-10°	0°	0.5	3.2	BT722-6314	BT721-6314
Edgewise	16/36	0°	0°	0.5	3.2	BT732-6311	BT731-6311
	26/46	0°	0°	0.5	3.2	BT732-6312	BT731-6312

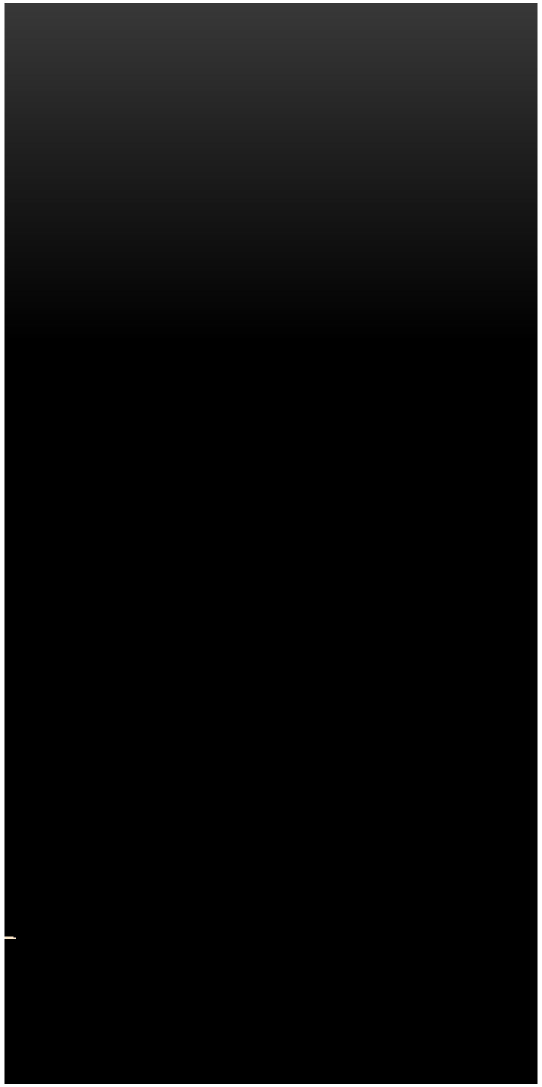

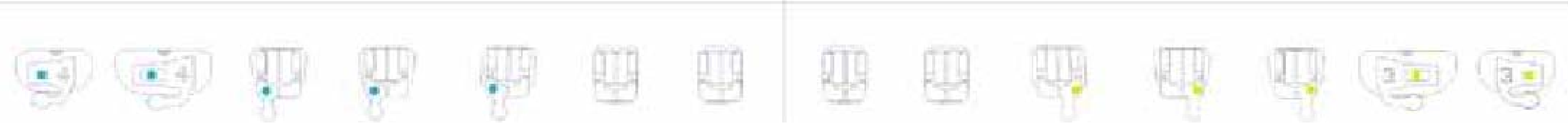

Torque			-22°	-17°	-11°	-1°	-1°	-1°	-1°	-11°	-17°	-22°
Tip			0°	0°	+5°	0°	0°	0°	0°	+5°	0°	0°
in/out mm			0.6	0.6	0.7	1.1	1.1	1.1	1.1	0.7	0.6	0.6
width mm			2.8	2.8	2.8	2.75	2.75	2.75	2.75	2.8	2.8	2.8
REF	18*	Senza gancio	BR821-10454	BR811-10444	BR811-10434	BR811-10314	BR811-10314	BR811-10314	BR811-10314	BR811-10334	BR811-10344	BR811-10354
		Con gancio	BR821-11454	BR811-11444	BR811-11434	-	-	-	-	BR811-11334	BR811-11344	BR811-11354
	22	Senza gancio	BR822-10454	BR812-10444	BR812-10434	BR812-10314	BR812-10314	BR812-10314	BR812-10314	BR812-10334	BR812-10344	BR812-10354
		Con gancio	BR812-11454	BR812-11444	BR812-11434	-	-	-	-	BR812-11334	BR812-11344	BR812-11354
Confezione			2	2	2	2	2	2	2	2	2	2

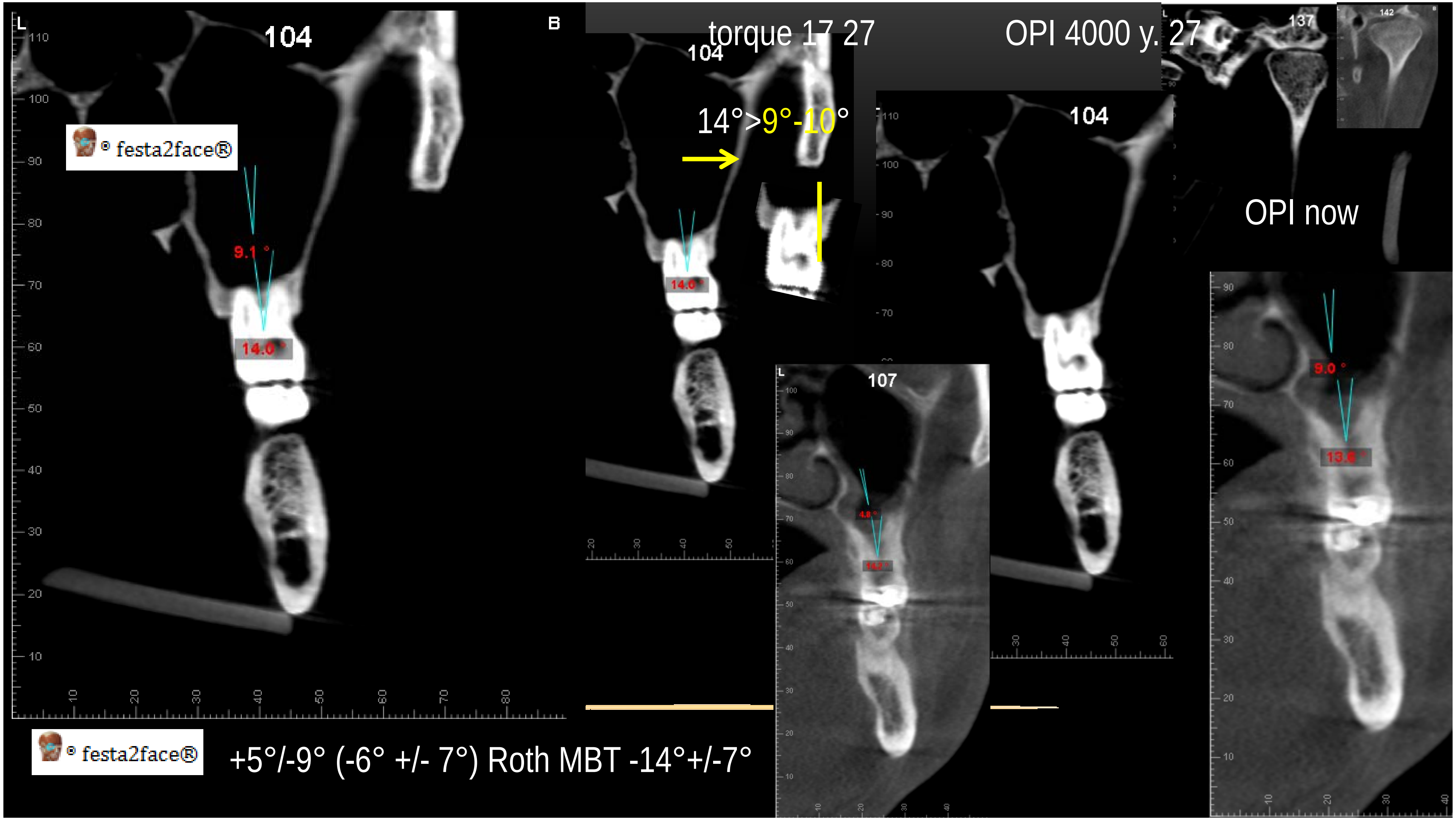
104
torque 17 27
OPI 4000 y. 27
137
142
® festa2face®
9.1 °
14.0 °
104
14°>9°-10°
14.0 °
104
107
OPI now
9.0 °
13.8 °
® festa2face®
+5°/-9° (-6° +/- 7°) Roth MBT -14°+/-7°

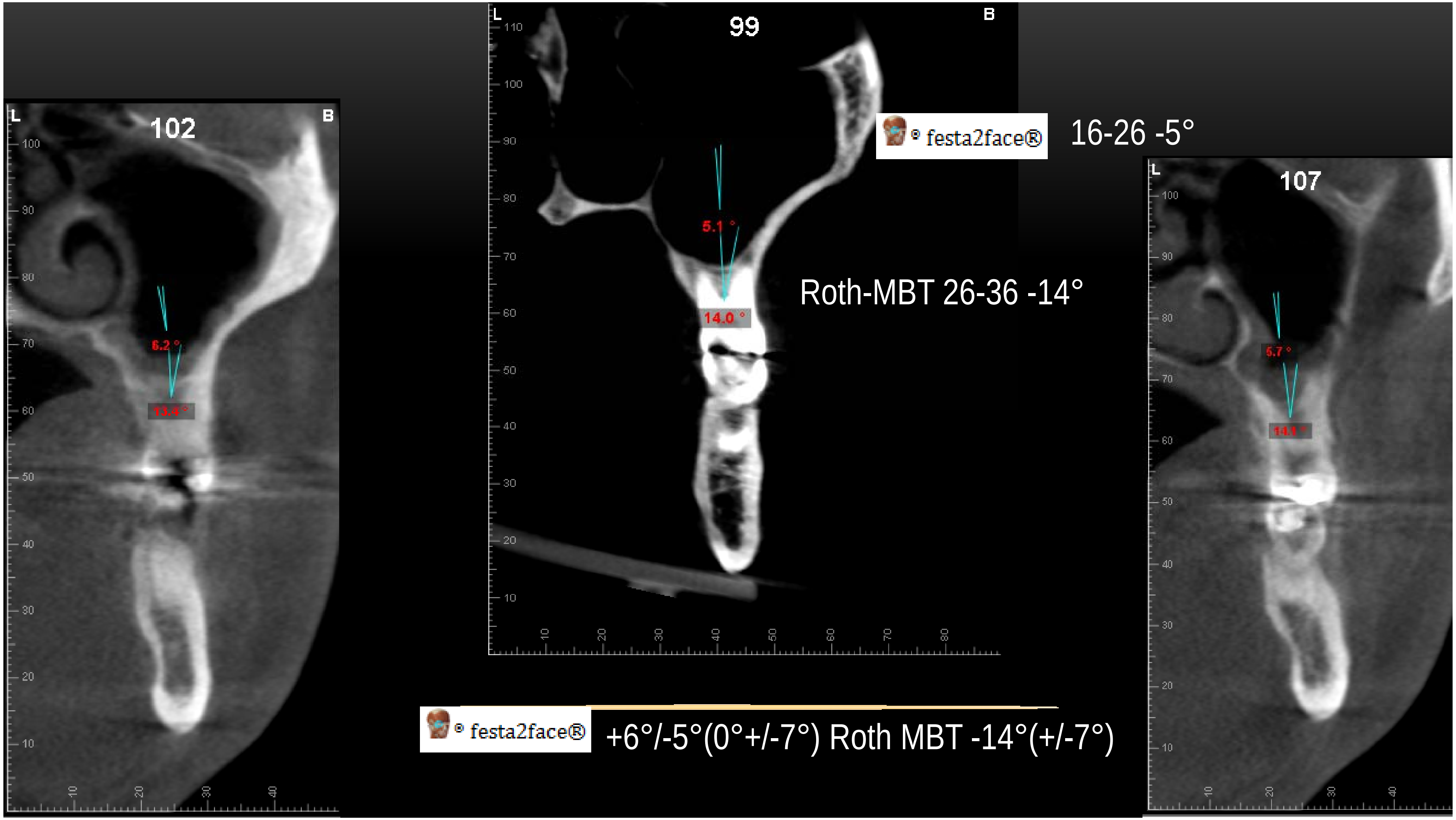

102
99
107
festa2face®
16-26 -5°
Roth-MBT 26-36 -14°
5.1 °
14.0 °
6.2 °
5.7 °
festa2face®
+6°/-5°(0°+/-7°) Roth MBT -14°(+/-7°)

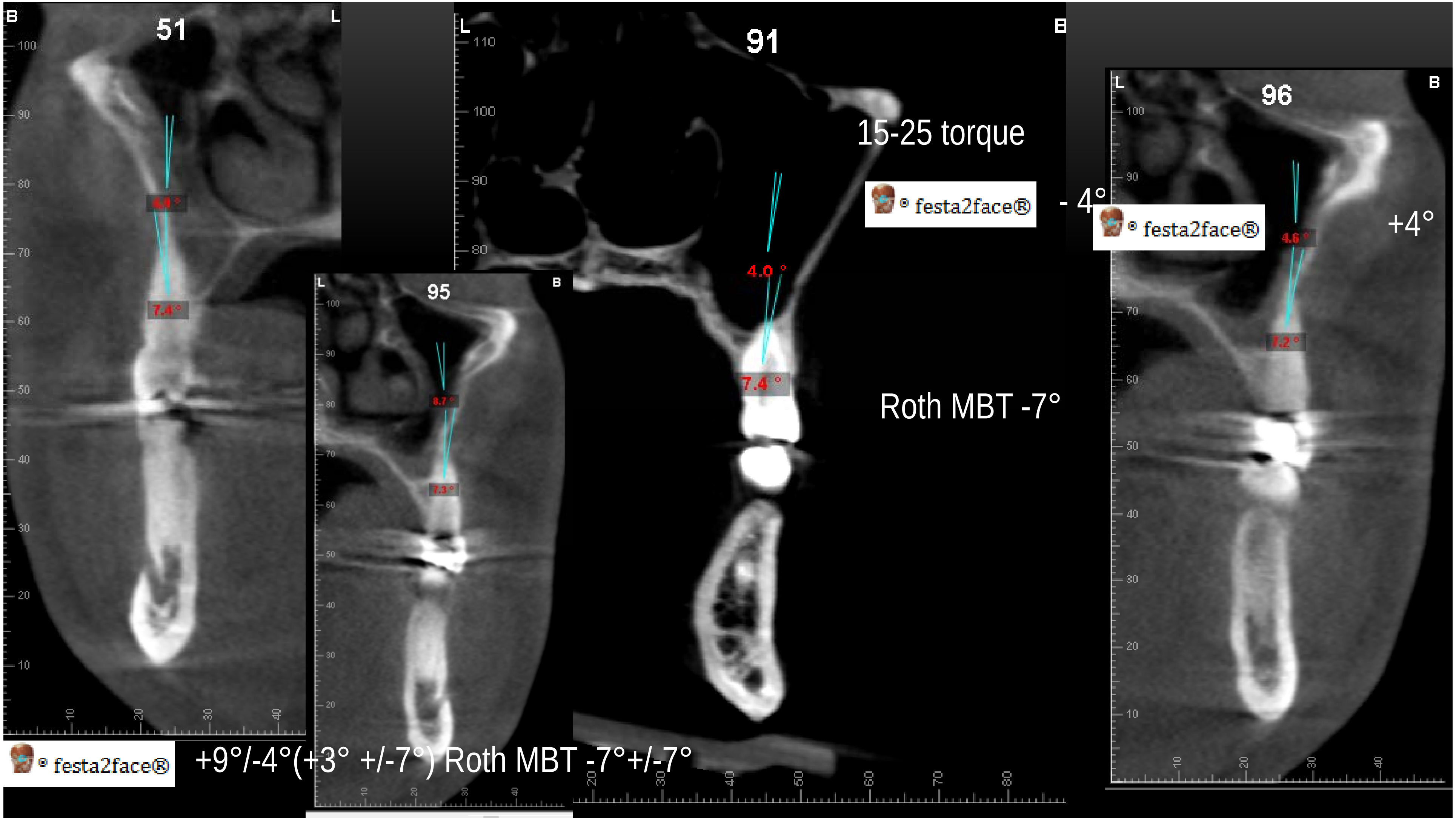
51
95
91
96
15-25 torque
festa2face®
- 4°
festa2face®
+4°
Roth MBT -7°
festa2face®
+9°/-4°(+3° +/-7°) Roth MBT -7°+/-7°

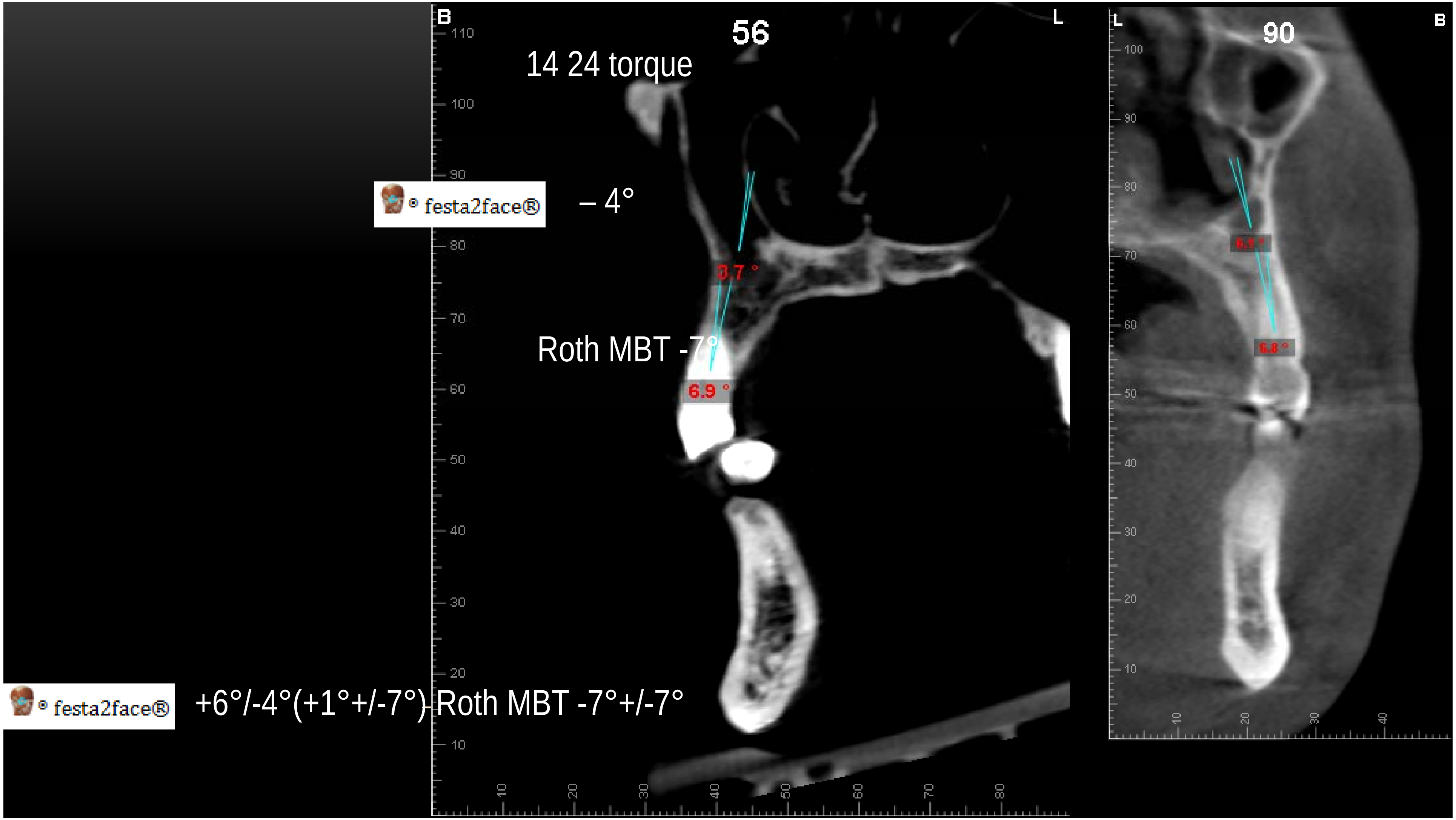

14 24 torque
56
90
– 4°
festa2face®
Roth MBT -7°
6.9 °
6.8 °
festa2face®
+6°/-4°(+1°+/-7°) Roth MBT -7°+/-7°

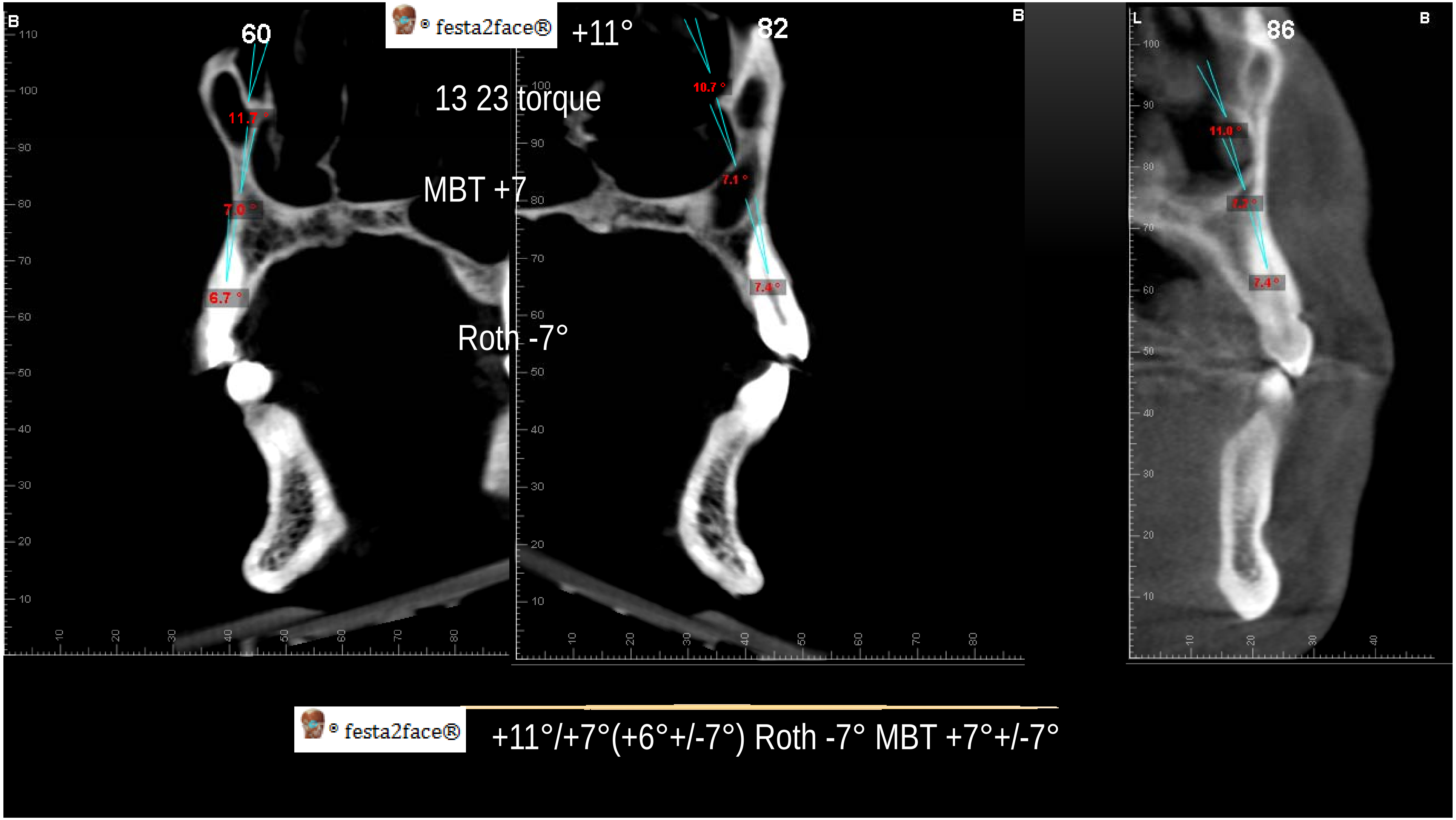
festa2face®
+11°
13 23 torque
MBT +7
Roth -7°
60
11.7 °
7.0 °
6.7 °
82
10.7 °
7.1 °
7.4 °
86
11.0 °
7.3 °
7.4 °
festa2face®
+11°/+7°(+6°+/-7°) Roth -7° MBT +7°+/-7°

12-22 torque

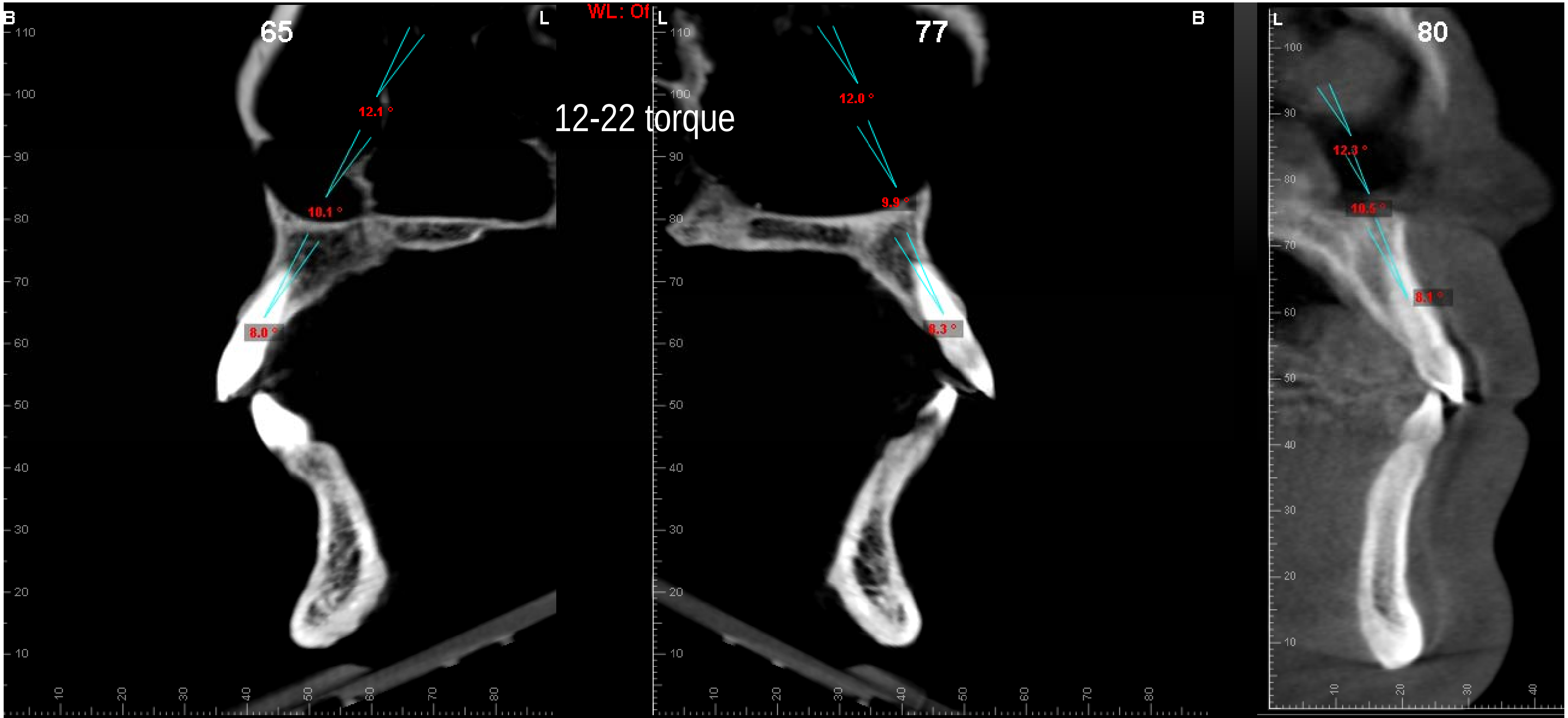

festa2face®

+12°/8°(10°+/-3°) Roth +8° MBT +10° (+/-3°)

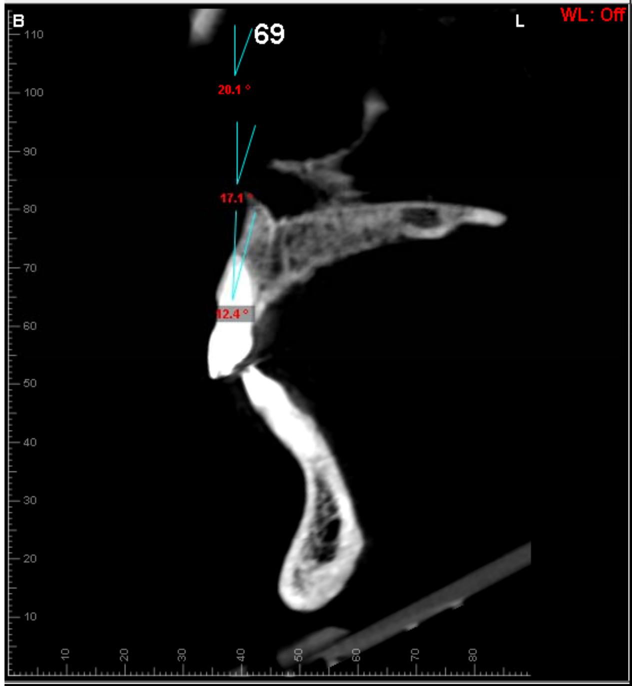

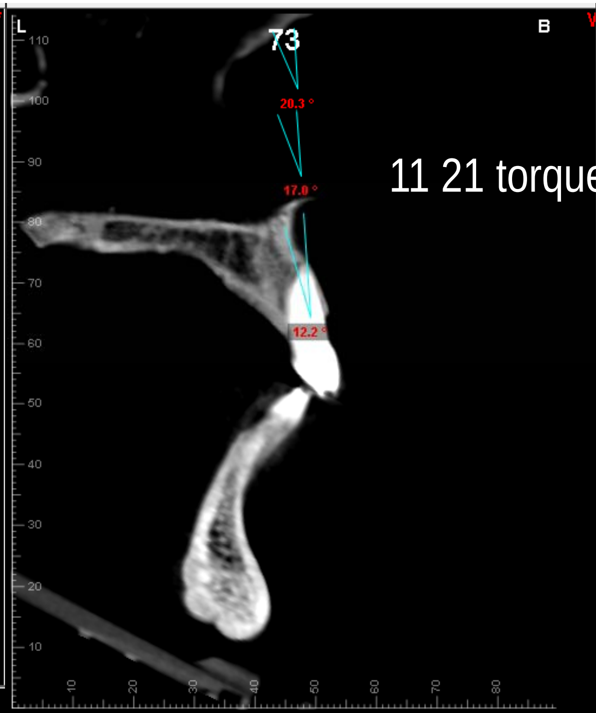

11 21 torque

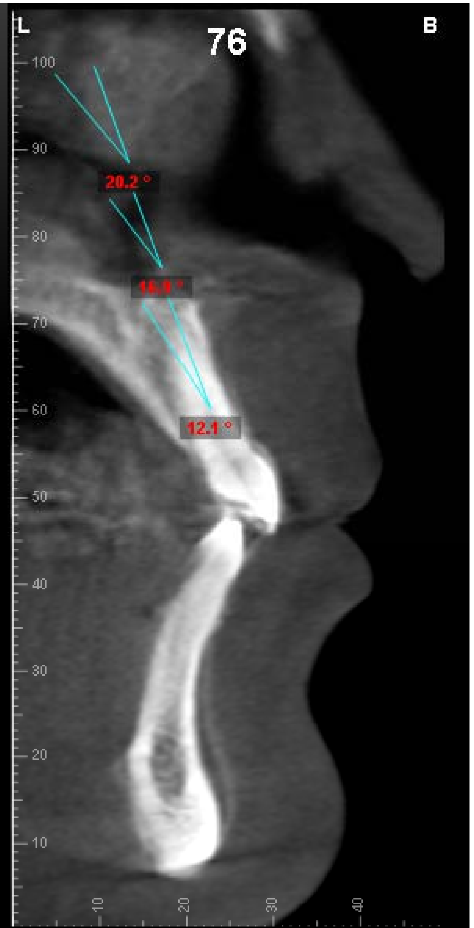

© festa2face®

+20°/+15°(17°+/-3°) Roth +12° MBT +17°(+/-3°)

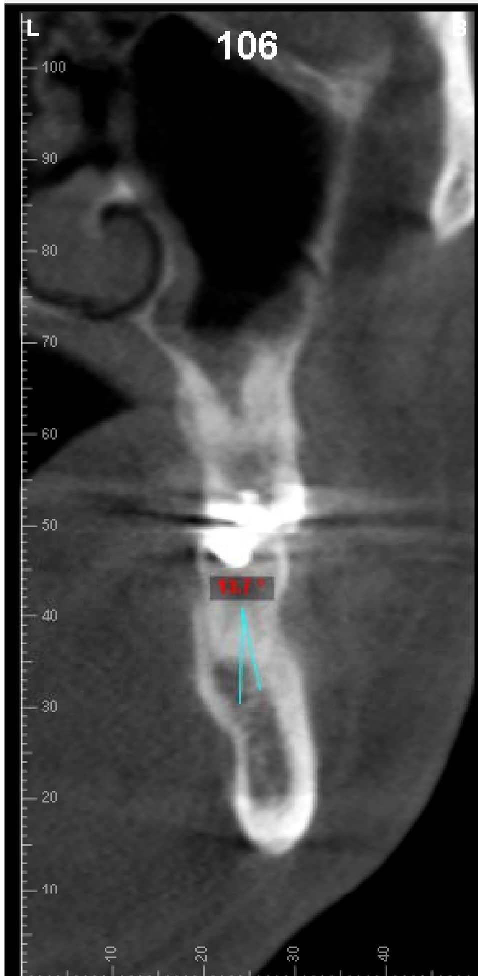

37 47 torque

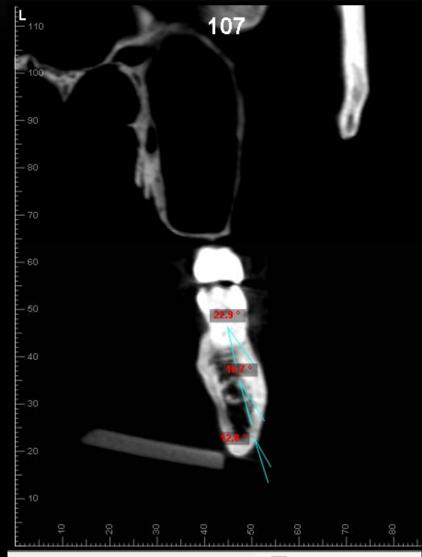

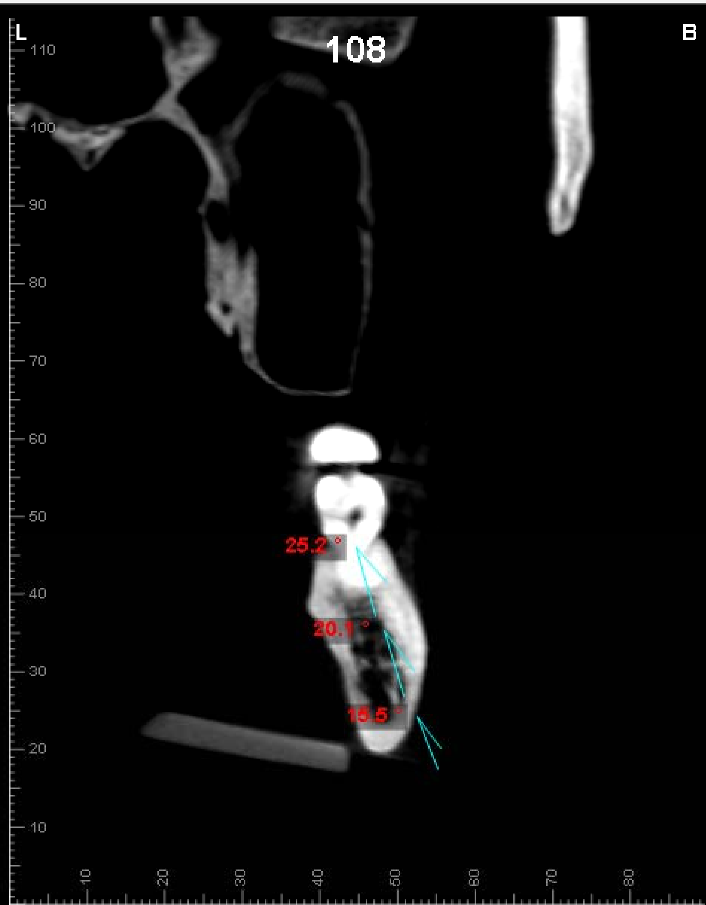

festa2face® -13°/-17°(-17°+/-8°) Roth -22°/-25° MBT -17°/-20°(+/-8°)

36 46 torque

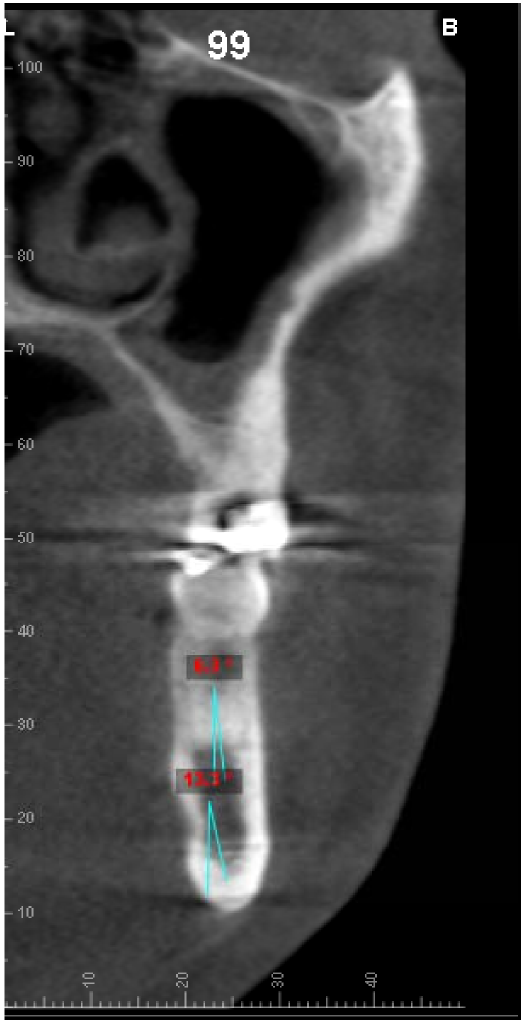

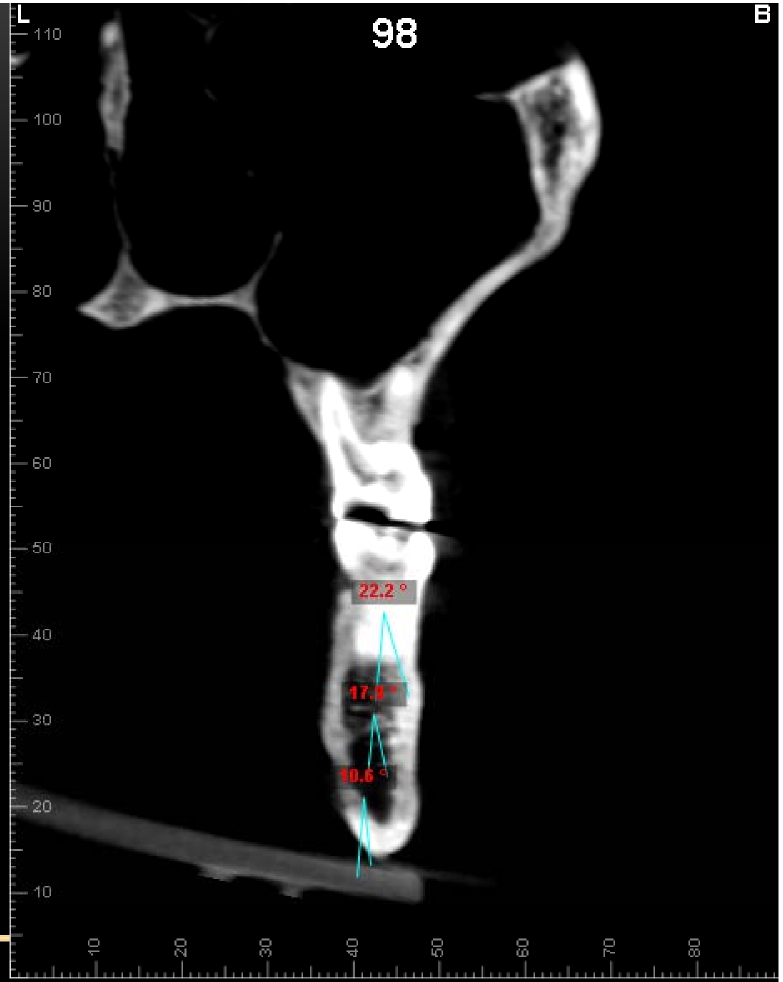

festa2face®

-6°/-13°(-13°+/-8°) Roth -22°/-25° MBT -17°/-20° +/-8°

35 45 torque

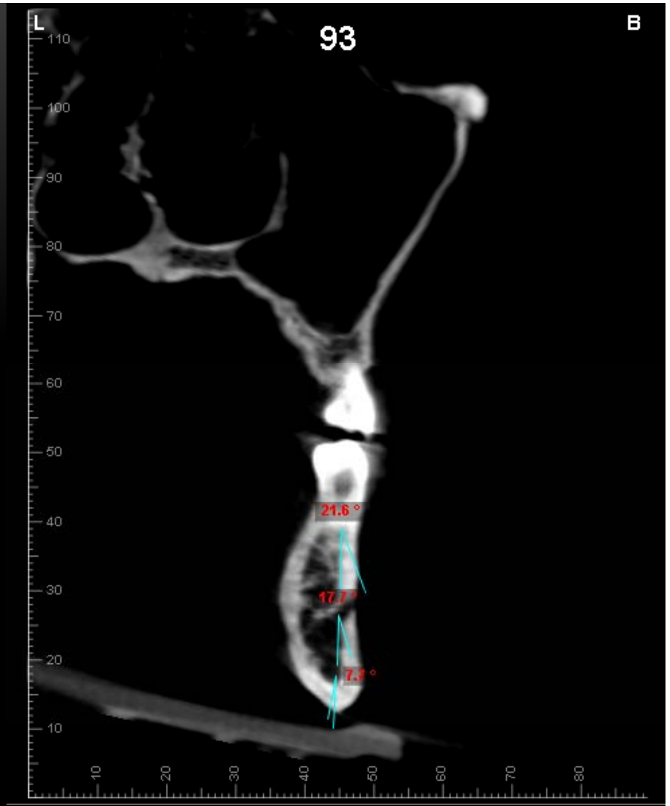

festa2face®

+3°/-10°(-10°+/-8°) Roth -22° MBT -17° +/-8°

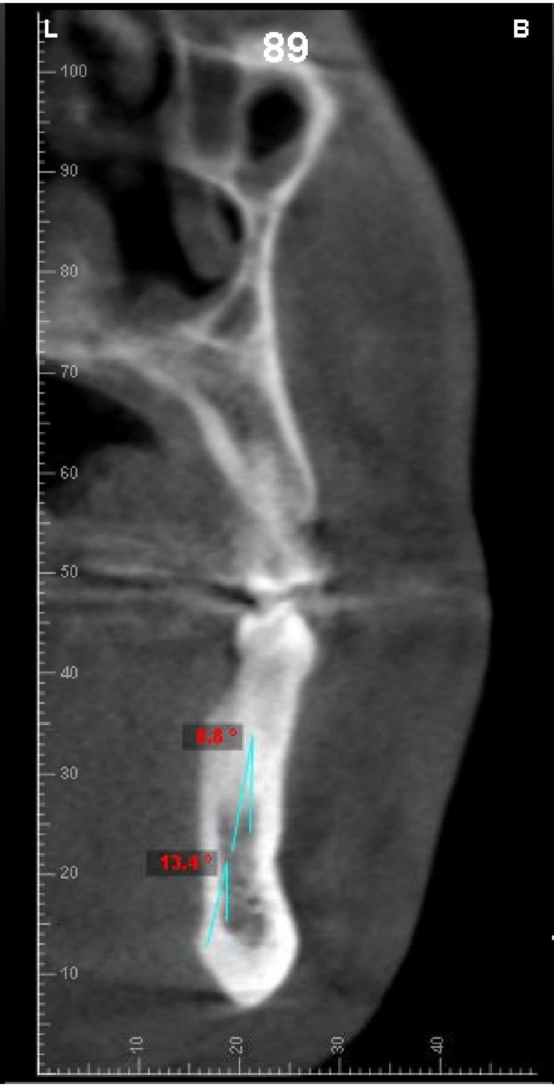

34 44 torque

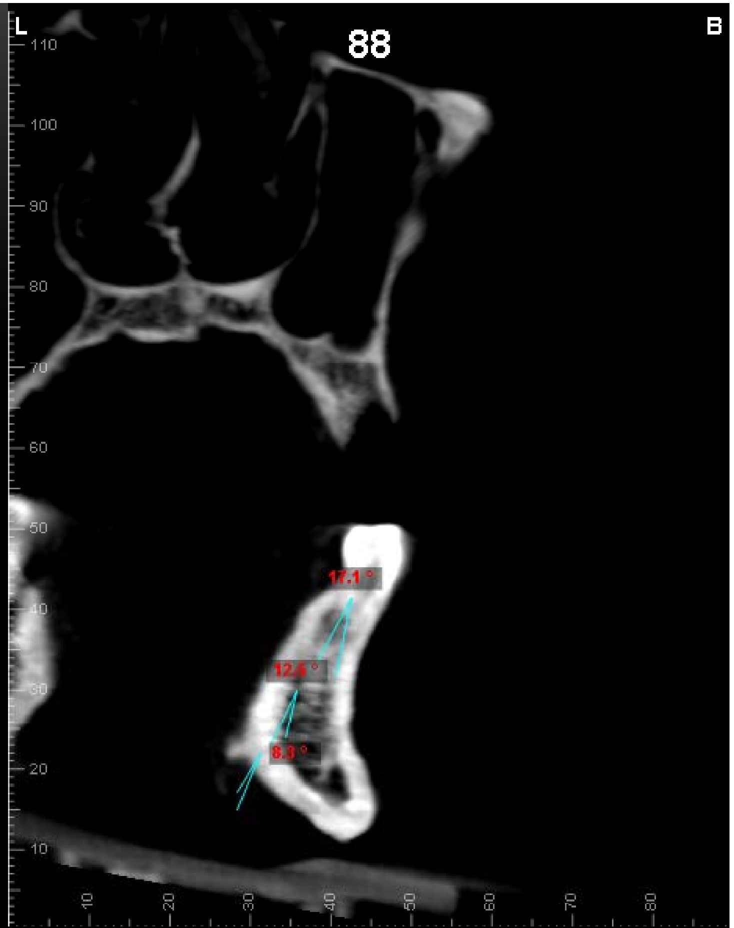

festa2face®

+3°/+8°/-8°/-14°(-9°+/-8°) Roth -17° MBT -12° +/-8°

33 43 torque

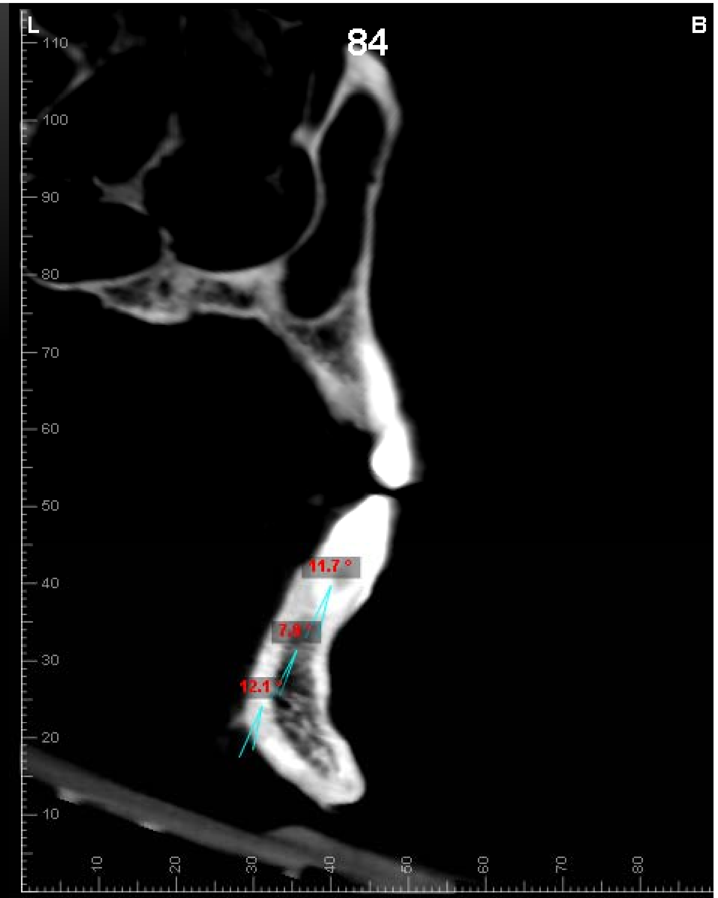

festa2face®

-10°/-11°/-13°/-15°(-11°+/-8°) Roth -11° MBT -6°(+/-8°)

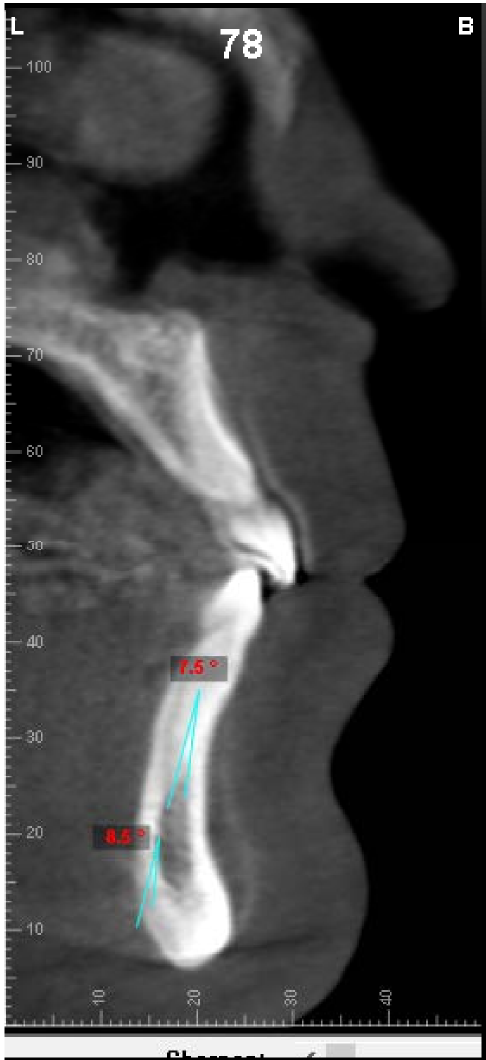

32 42 torque

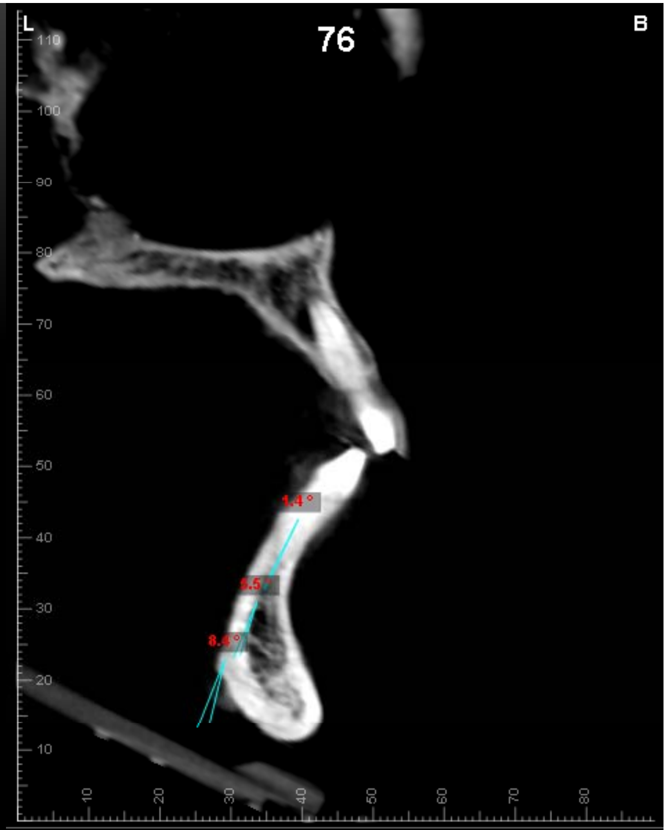

® festa2face®

-6°/-8°/-9°(-6°+/-8°) Roth -1° MBT -6°+/-8°

31 41 torque

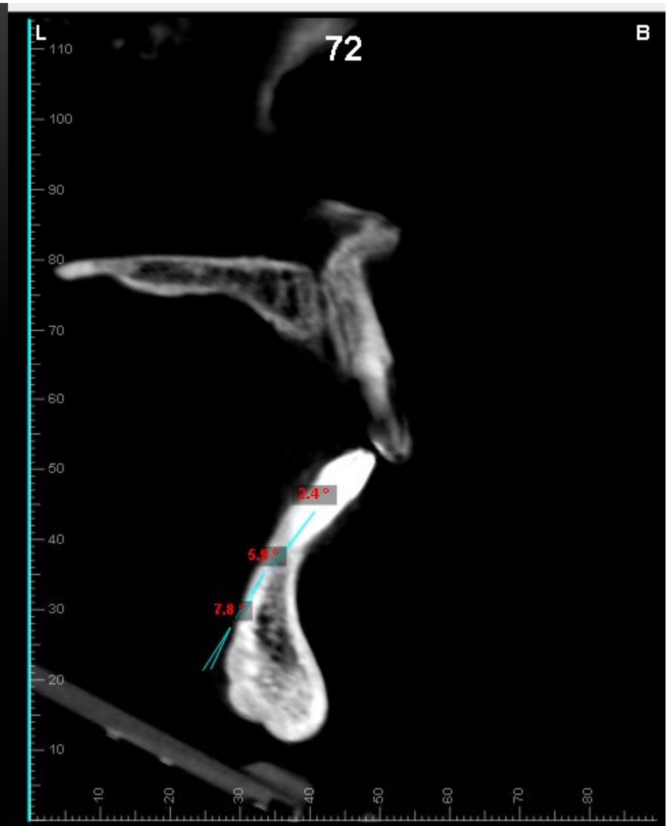

festa2face®

-6°/-8°/-9°(-6°+/-8°) Roth -1° MBT -6°+/-8°

TECNICA MBT

Il kit comprende i tubi per I e II molare

Torque			-7°	-7°	-7°	+10°	+17°	+17°	+10°	-7°	-7°	-7°
Tip			0°	0°	+8°	+8°	+4°	+4°	+8°	+8°	0°	0°
in/out mm			0,8	0.8	0.8	1.15	0.9	0.9	1.15	0.8	0.8	0.8
width mm			2.8	2.8	2.8	2.75	3.0	3.0	2.75	2.8	2.8	2.8
REF	18*	Senza gancio	BR821-10144	BR821-10144	BR821-10134	BR821-10124	BR821-10114	BR821-10214	BR821-10224	BR821-10234	BR821-10244	BR821-10244
		Con gancio	BR821-11144	BR821-11144	BR821-11134	-	-	-	-	BR821-11234	BR821-11244	BR821-11244
	22	Senza gancio	BR822-10144	BR822-10144	BR822-10134	BR822-10124	BR822-10114	BR822-10214	BR822-10224	BR822-10234	BR822-10244	BR822-10244
		Con gancio	BR822-11144	BR822-11144	BR822-11134	-	-	-	-	BR822-11234	BR822-11244	BR822-11244
Confezione			2	2	2	2	2	2	2	2	2	2

Mandibolare

Mascellare

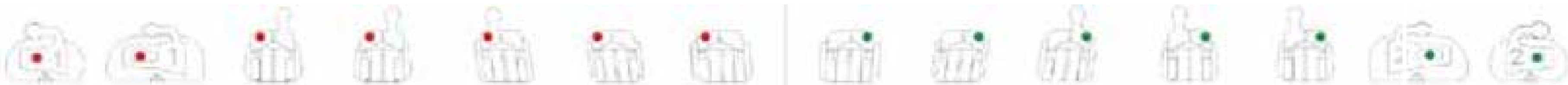

Brackets Se

WePass™

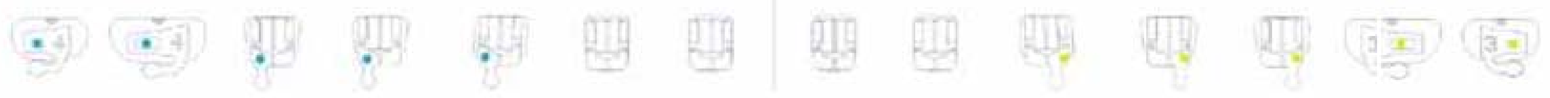

Torque			-17°	-12°	-6°	-6°	-6°	-6°	-6°	-6°	-12°	-17°
Tip			0°	0°	+3°	0°	0°	0°	0°	+3°	0°	0°
in/out mm			0.8	0.8	0.8	1.15	1.15	1.15	1.15	0.8	0.8	0.8
width mm			2.8	2.8	2.8	2.76	2.76	2.76	2.76	2.8	2.8	2.8
REF	18*	Senza gancio	BR821-10454	BR821-10444	BR821-10434	BR821-10314	BR821-10314	BR821-10314	BR821-10314	BR821-10334	BR821-10344	BR821-10354
		Con gancio	BR821-11454	BR821-11444	BR821-11434	-	-	-	-	BR821-11334	BR821-11344	BR821-11354
	22	Senza gancio	BR822-10454	BR822-10444	BR822-10434	BR822-10314	BR822-10314	BR822-10314	BR822-10314	BR822-10334	BR822-10344	BR822-10354
		Con gancio	BR822-11454	BR822-11444	BR822-11434	-	-	-	-	BR822-11334	BR822-11344	BR822-11354
Confezione			2	2	2	2	2	2	2	2	2	2

SLOT	Contenuto	Conf	3° con gancio	3°/4°/5° con gancio
18	1 Kit	28 pcs	BR821-134	BR821-154
22	1 Kit	28 pcs	BR822-134	BR822-154

Torque differenziali

Superiore	Centrale		Laterale		Canino	
	-	+	-	+	-	+
	+5°	+22°	-3°	+13°	+0°	+7°

Inferiore	Laterale		Canino	
	-	+	+	
	-10°	+3°	-0°	+7°

TECNICA ROTH

Il kit comprende i tubi per I e II molare

Torque	-7°	-7°	-2°	+8°	+12°	+12°	+8°	-2°	-7°	-7°

Torque	-22°	-17°	-11°	-1°	-1°	-1°	-1°	-11°	-17°	-22°

16/26	17/27
↓	↓
-14°	-14°
-25°	-25°
↑	↑
36/46	37/47

TECNICA festa2face®

Il kit comprende i tubi per I e II molare

Torque	+9°/+3°	+9°/+1°	+11°/+6°	+12°/+10°	+15°/+17°	+15°/+17°	+12°/+10°	+11°/+6°	+9°/+1°	+9°/+3°

festa2face® Torque	-10°/-9°	-8°/-9°	-13°/-11°	-8°/-6°	-8°/-6°	-8°/-6°	-8°/-6°	-13°/-11°	-8°/-9°	-10°/-9°

-5°/0°	-9°/-6°
-6°/-10°	-13°/-17°

TECNICA MBT

Il kit comprende i tubi per I e II molare

Torque	-7°	-7°	-7°	+10°	+17°	+17°	+10°	-7°	-7°	-7°

Torque	-17°	-12°	-6°	-6°	-6°	-6°	-6°	-6°	-12°	-17°

-14°	-14°
-20°	-10°

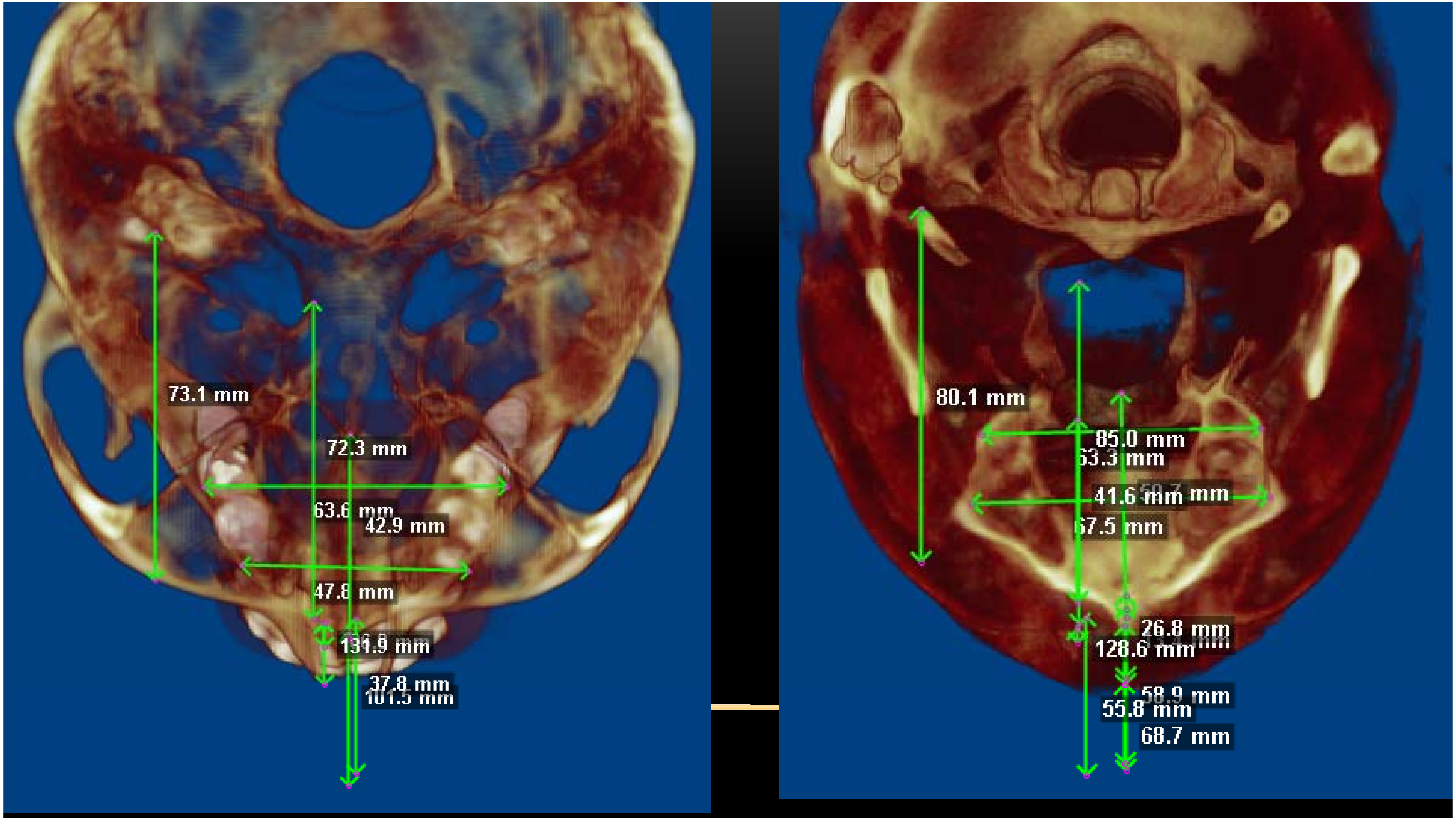
73.1 mm
72.3 mm
63.6 mm
42.9 mm
47.8 mm
131.9 mm
37.8 mm
101.5 mm
80.1 mm
85.0 mm
41.6 mm
26.8 mm
128.6 mm
58.9 mm
55.8 mm
68.7 mm

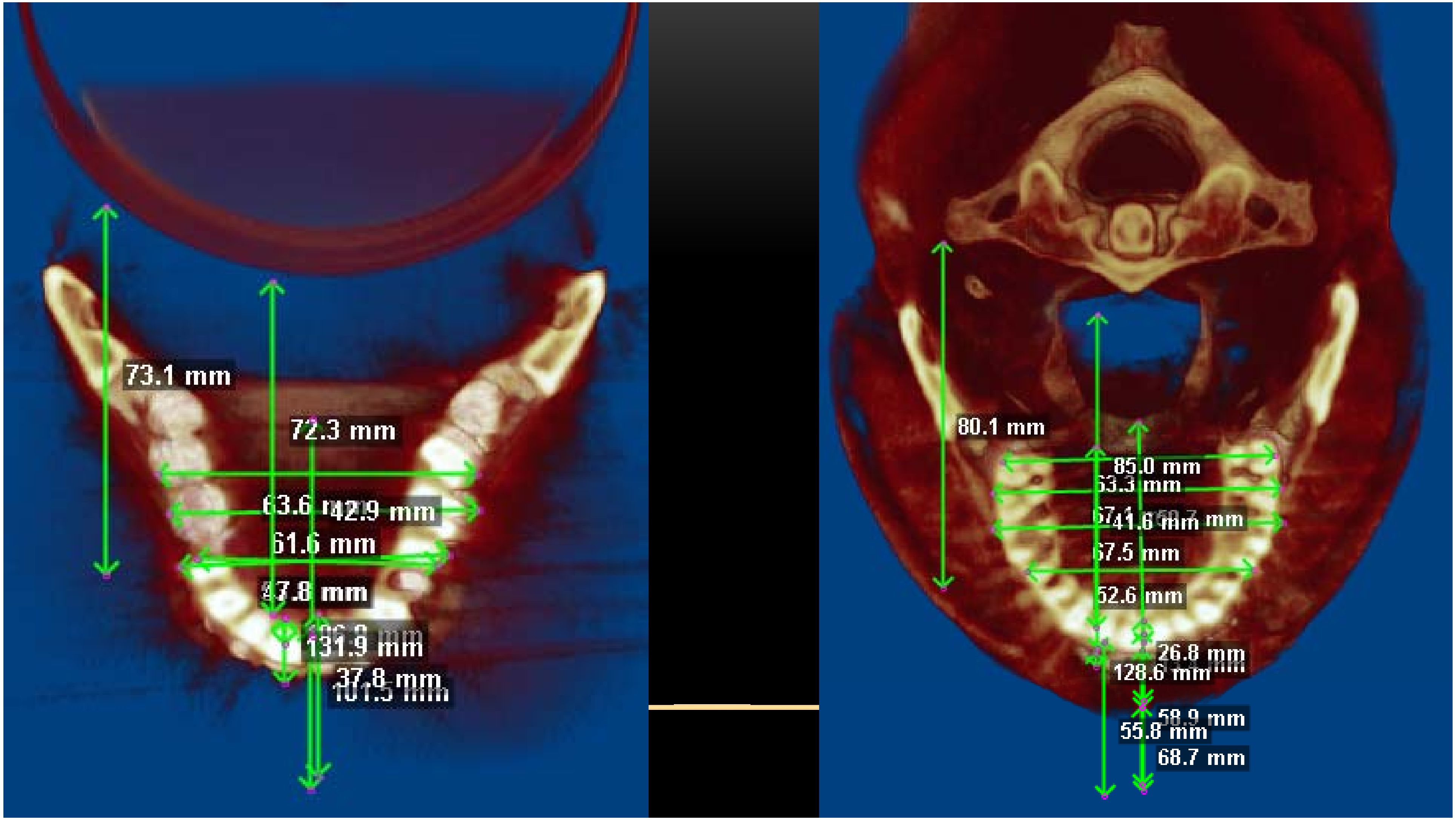

73.1 mm
72.3 mm
42.9 mm
61.6 mm
131.9 mm
37.8 mm
80.1 mm
85.0 mm
52.6 mm
26.8 mm
128.6 mm
58.9 mm
55.8 mm
68.7 mm

Asiatic Homo Erectus

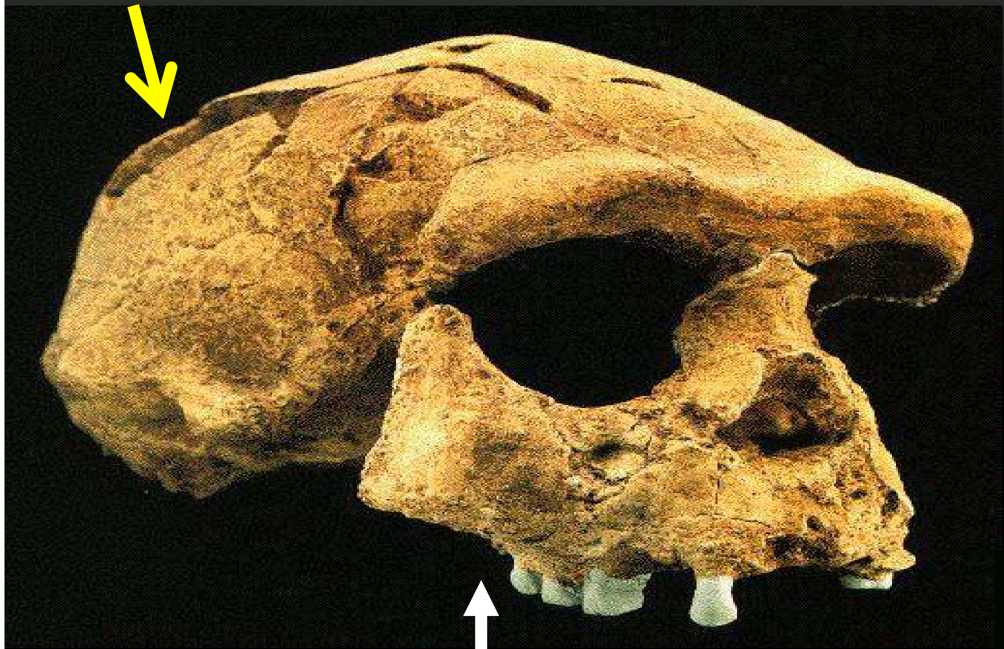

Caucasic Homo Erectus

Sangiran 17, "Pithecanthropus VIII", *Homo erectus*
Discovered by Sastrohamidjojo Sartono in 1969 at Sangiran on Java. This consists of a fairly complete cranium, with a brain size of about 1000 cc. It is the most complete *erectus* fossil from Java. <u>This skull is very robust, with</u>

IN ASIA Hominids had a flatter and larger maxilla related to Caucasians

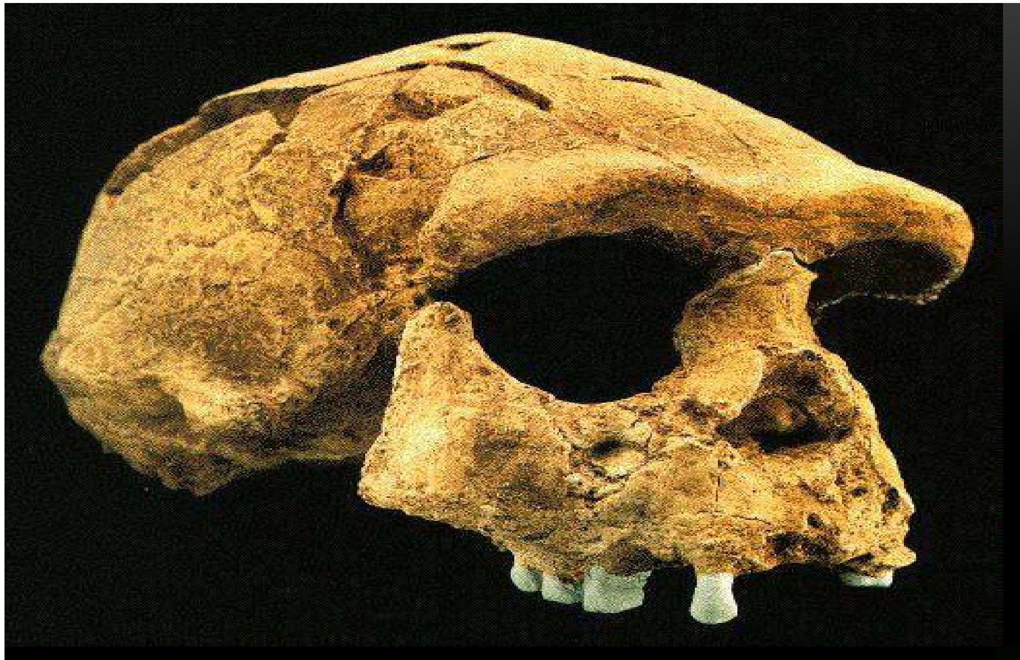

...ANCHE SE GLI OMINIDI DIFFERISCONO TRA LE VARIE AREE

Sangiran 17, "Pithecanthropus VIII", *Homo erectus*
Discovered by Sastrohamidjojo Sartono in 1969 at Sangiran on Java. This consists of a fairly complete cranium, with a brain size of about 1000 cc. It is the most complete *erectus* fossil from Java. This skull is very robust, with

↑

ASIAN HOMINIDS HAD A FLATTER AND LARGER MAXILLA

GENOMIC ANTHROPOLOGY IS THE TRAIN TO BRING STEM CELLS THERAPY INSIDE HUMAN FACE

Felice Festa